Defining the maximum extent of the Laurentide Ice Sheet in Home Bay (eastern Arctic Canada) during the Last Glacial episode

YAN LÉVESQUE, GUILLAUME ST-ONGE, PATRICK LAJEUNESSE, PIERRE-ARNAUD DESIAGE AND ETIENNE BROUARD

Three sediment cores recovered on the lower slope of the continental shelf in western Baffin Bay (Arctic Canada) as well as swath bathymetry and subbottom profiler data collected on the shelf and slope of the region were analyzed to investigate if the Laurentide Ice Sheet (LIS) reached the shelf edge offshore Home Bay during the Last Glacial Maximum (LGM). Physical, sedimentological, and palaeomagnetic analyses of the cores were also used to constrain the chronostratigraphy of upper sedimentary facies of the Home Bay trough-mouth fan (TMF). Seven lithofacies were identified in the cores and reveal that the sediments recorded a genuine geomagnetic signal and that the cores span the last 40 ka. In the Home Bay Trough, sets of elongated ridges are discernable on swath bathymetry imagery and are interpreted as mega-scale glacial lineations (MSGLs) resulting from an ice stream eroding the trough and delivering glaciogenic sediments to the TMF. The geomorphology of the TMF, combined with the sedimentary records and the chronostratigraphy, indicates that a series of debris flows and turbidity currents were generated between 35 and 15 ka BP. These results indicate that the LIS margin extended near the shelf edge during the LGM and allow us to propose a new maximum extent of the LIS during the Last Glacial episode.

Yan Lévesque (yan.levesque@uqar.ca), Guillaume St-Onge and Pierre-Arnaud Desiage, Institut des sciences de la mer de Rimouski (ISMER), Canada Research Chair in Marine Geology, Université du Québec à Rimouski and

GEOTOP, 310 allée des Ursulines, Rimouski, QC, Canada, G5L 3A1; Patrick Lajeunesse, Département de géographie and Centre d'études nordiques, Université Laval, QC, Canada, G1V 0A6; Étienne Brouard, Département des sciences de la Terre et de l'atmosphère, Université du Québec à Montréal, QC, Canada, H3C 3P8.

The Laurentide Ice Sheet (LIS) covered most of North America during the last glaciation and the eastern margin of Baffin Island, in the eastern Canadian Arctic, has been shaped by its phases of advance and retreat (Dyke & Prest 1987; Dyke 2004). Therefore, Baffin Bay, located between Baffin Island and Greenland, forms a unique setting capturing sediments related to the pulses of ice sheet margins on the surrounding continental shelves (e.g. Simon *et al.* 2012, 2014, 2016; Brouard & Lajeunesse 2017; Jenner *et al.* 2018). Recent studies have suggested that the LIS margin extended on the northeastern Baffin Island shelf during the Last Glacial Maximum (LGM) and reached the shelf edge (Fig. 1A, B; Li *et al*. 2011; Brouard & Lajeunesse 2017; Jenner *et al*. 2018). These studies contrast with the generally accepted LIS extent and chronologies which portray the LIS as only extending few kilometers seaward of the mouth of the fiords (Briner *et al.* 2005, 2006). According to Dyke *et al*. (2002) ice only began to recede from its maximum position (e.g. fiord mouths) around 13-12 ka BP.

Ice sheet dynamics near a shelf edge can generate considerable temporal and spatial variability in the depositional processes of glaciogenic sediments onto the continental slope and in ocean basins (Laberg & Vorren 1995; King *et al*. 1998; Vorren *et al*. 1998; Nygard *et al*. 2002). A range of sedimentary processes have been described and include glaciogenic debris flows (GDFs) and turbidity currents, which flow through canyons and gullies, and can accumulate tens to hundreds of kilometers downslope on submarine deep sea fans (e.g. TMFs; Ó Cofaigh *et al*. 2003; De Blasio *et al*. 2004; Laberg & Vorren 1995; Vorren *et al*. 1998; Tripsanas & Piper 2008). TMFs are generally composed of stacked glaciogenic debrites that in some cases alternate laterally with turbidites also of glacial origin; they can therefore be used to identify periods of glacial activity at the shelf edge (e.g. Laberg & Vorren 1995; Vorren *et al*. 1998; Tripsanas & Piper 2008). Establishing the temporal evolution setting of the sediment accumulation within a TMF can, however, be highly challenging due to chronostratigraphic limitations. Indeed, datable material such as biogenic carbonates are scarce and/or not well-preserved in the Canadian Arctic, especially in Baffin Bay (de Vernal *et al*. 1987, 1992 ; Ledu *et al*. 2008; McKay *et al*. 2008; Simon *et al*. 2012). To circumvent these issues, palaeomagnetism combined with radiocarbon dating can provide an age control on the glaciogenic triggering events (Stoner & St-Onge 2007; St-Onge & Stoner 2011). Sediment cores taken offshore of high-latitude continental margins are particularly well suited for high-resolution Quaternary palaeoenvironmental reconstructions and can provide continuous and reliable records of variations in the geomagnetic field (e.g. Andrews & Jennings 1990; Snowball & Sandgren 2002; Snowball & Muscheler 2007; Barletta *et al*. 2008).

Here, we present a palaeomagnetic sequence of the relative palaeointensity from the continental margin of Baffin Island and compare this sequence to one palaeomagnetic record (Simon *et al*. 2012) and two others palaeomagnetic stacks from the North Atlantic and Mediterranean Sea/Somalian Basin (Meynadier *et al*. 1992; Laj *et al*. 2000) to obtain a time frame for the cores collected from Home Bay TMF, in order to determine if the LIS reached the self edge during the LGM. In addition, we use swath bathymetry and subbottom profiler data to identify landforms and deposits left by the LIS on the Home Bay cross-shelf trough and fan.

Regional setting

Baffin Bay forms a narrow (450 km-wide) oceanic basin located between the Canadian Arctic Archipelago and Greenland that is characterized by an anticlockwise ocean circulation (West Greenland and Baffin Island currents; Fig. 1A) and by partial sea ice cover during most of the year (Tang *et al*. 2004). Archaean and Palaeoproterozoic cratons form the main geological units on either side of Baffin Bay, and are overlain by a succession of Palaeozoic rocks dominated by shallow carbonates such as dolostones and limestones (Aksu & Piper 1987; Hiscott *et al*. 1989; Simon *et al*. 2012; Stanley & Luczaj 2015).

During the LGM, Baffin Bay was surrounded by three major ice sheets that flowed into it: the Greenland Ice Sheet (GIS), the Laurentian Ice Sheet (LIS) and the Innuitian Ice Sheet (IIS) (Dyke & Prest 1987; Dyke *et al*. 2002; Stokes 2017). The LIS extended across Baffin Island and possibly covered much of the fiords and the continental shelf (Briner *et al*. 2006; Funder *et al*. 2011). Quaternary deposits from Baffin Bay, mainly debris flows and turbidites, also suggest that the LIS may have reached the Baffin Island continental shelf during the LGM (Aksu & Piper 1987; Hiscott & Aksu 1994; Praeg *et al*. 2006). These turbidites and debrites relate to meltwater processes that periodically incised canyons and submarine valleys on TMFs (e.g. Tripsanas & Piper 2008; Li *et al.* 2012). Therefore, they record periods of ice occupying the troughs. Basal diamictons are often observed in sediment cores collected on the NE Baffin slope near the mouths of TMFs (Table 1, Fig. 2). They usually represent GDFs that were triggered by glacial advance during the LGM (Jenner *et al*. 2018). Deglaciation of the LIS in Baffin Bay is thought to have begun around 16-15 cal. ka BP, but only beginning around 13-12 cal. ka BP in Home Bay (Dyke & Prest 1987; Dyke *et al*. 2002; Dyke 2004).

Material and methods

Sediment cores

Two piston cores and one large square gravity core (CASQ) were collected with their companion trigger weight cores (TWC) and associated box cores (BC) in central Baffin Bay in 2016 and 2017. Cores AMD16-LGM-09 and AMD0217-01, hereinafter referred as cores 9CASQ and 1Comp, were collected aboard the CCGS Amundsen from the Home Bay TMF; core HU2013-029-0077 (hereinafter referred as 77PC) was collected in 2013 aboard the CCGS Hudson during cruise 2013029 with the purpose of serving as a chronostratigraphic reference core (Table 1, Fig. 1; Campbell 2014).

Seismo-stratigraphy and swath bathymetry

High-resolution swath bathymetry data were acquired using a hull-mounted Kongsberg EM-302 (30 kHz) echosounder. High-resolution acoustic subbottom data were collected with a Knudsen 3.5 kHz Chirp system and analyzed using The Kingdom Suite software (IHS). Subbottom profiles were analyzed onboard in order to identify areas of Quaternary sedimentary sequences in which mass movements and/or sediment perturbations were present inside the TMF (i.e. the coring sites). The geomorphology of the Home Bay area was mapped by the interpretation of the swath bathymetric data that were processed using the CARIS HIPS and SIPS software and then visualized with the QPS Fledermaus software. Finally, airgun seismic reflection data (Line 76029_AG_280_1730) were acquired through the public database of the National Resources Canada Marine Data Holdings. The airgun data were used to investigate the sedimentary architecture of the cross-shelf trough in search of potential grounding-zone wedges (GZW) in the area.

Physical and geochemical properties

To define the stratigraphy and sedimentary facies, sections of core 9CASQ were passed through a computerized axial tomography scanner (CAT-Scan) at the Institut national de la recherche scientifique, Centre Eau Terre Environnement (INRS-ETE) in Québec City to characterize the sedimentary facies and sediment structures (St-Onge *et al*. 2007). Similarly, the sections of core 1Comp were scanned with a GEOTEK XCT digital X-ray system at ISMER (Fig. 2). Whole cores were then analyzed using the GEOTEK Multi Sensor Core Logger (MSCL) at 1 cm intervals to measure the low-field volumetric magnetic susceptibility (k_{LF}) and the wet bulk density using gamma-ray attenuation; then, the core was split, described and photographed. Diffuse spectral reflectance was then acquired with an online Minolta CM-2600d spectrophotometer at 0.5 cm intervals, while the concentration of minor and major chemical elements (calcium (Ca), strontium (Sr), iron (Fe), Rubidium (Rb), among others) were determined by X-ray fluorescence (XRF) spectrometry for the same intervals using an Olympus Innov-X Handheld Delta XRF analyser Delta Family integrated to the MSCL. The grain size analysis was performed at 10 cm intervals on bulk sediment samples at ISMER using a Beckman Coulter™ LS13320 laser diffraction grain size analyzer, as well as at a higher resolution in specific facies such as in turbidites. Prior to analyses, samples were sieved at 2 mm. Apart from a few intervals with a few pebbles, no material larger than 2 mm was recovered. Therefore, the size fraction larger than 2 mm has been excluded from the grain size metrics.

Palaeomagnetic analysis

Palaeomagnetic data were measured at 1 cm intervals on u-channel samples (2 x 2 x 150 cm) using a 2G Enterprises™ cryogenic magnetometer at ISMER for chronostratigraphic purposes

139 and to identify possible rapidly deposited layers such as turbidites and debrites, which are characterized by low quality palaeomagnetic data and shallow inclinations (e.g. St-Onge *et al*. 2004; Tanty *et al*. 2016). The measurements performed were as follows: natural remanent magnetization (NRM), anhysteretic remanent magnetization (ARM), isothermal remanent magnetization (IRM) and saturation isothermal magnetization (SIRM). Due to the finite spatial resolution of the pick-up coils that integrates measurements over ~7–8 cm (Philippe *et al*. 2018), some smoothing occurred. To eliminate the edge effect associated with this response function, the data from the first and last 4 cm of each u-channel were excluded.

The NRM was measured and then progressively demagnetized using stepwise alternating field demagnetization (AF) at peak fields from 0 to 75 mT at 5 mT increments. Directions (inclination and declination) of the characteristic remanent magnetization (ChRM) were calculated using the Excel spreadsheet developed by Mazaud (2005) with AF demagnetization steps from 10 to 60 mT (11 steps) for the three cores. This method also provides maximum angular deviation (MAD) values, which are indicative of high-quality directional data for Quaternary palaeomagnetic studies if the MAD is lower than 5° (Stoner & St-Onge 2007). Using this spreadsheet, the median destructive field (MDF) of the NRM is also calculated. The MDF represent the required demagnetization field necessary to reduce the initial magnetic remanence by half of its initial intensity. The MDF is an indicator of magnetic mineralogy, reflects the mean coercivity state of the magnetic grain assemblage and depends on both the grain size and the mineralogy (e.g. Stoner & St-Onge 2007; Barletta *et al*. 2010) The ARM was then induced using a 100 mT AF with a 0.05 mT direct current (DC) biasing field. The ARM was then demagnetized and measured from 0 to 75 mT at every 5 mT. Two IRMs were imparted with a DC field of 0.3 T (IRM) and 0.95 T (SIRM) using a 2G Enterprises pulse magnetizer. Each IRM was measured from 0 to 75 mT at 5 mT demagnetization step increments; the steps used in the SIRM were 0, 10, 30, 50 and 70 mT.

To define the magnetic mineralogy, hysteresis measurements were performed at 10 cm intervals on a small quantity of sediment from the three cores using a Princeton Measurement Corporation MicroMag 2900 alternating gradient force magnetometer (AGM). The saturation magnetization (Ms), the coercive force (Hc), the saturation remanence (Mrs) and the coercivity of remanence (Hcr) were extracted from the hysteresis data to characterize the magnetic mineralogy and grain size (Day *et al*. 1977).

Radiocarbon dating

To develop the chronology of the cores, ^{14}C ages were obtained by accelerator mass spectrometry (AMS) on six samples from mixed planktonic and benthic foraminifera and one sample derived from *Neogloboquadrina pachyderma* shells (Table 2) at the Laboratoire des sciences du climat et de l'environnement (LSCE), Gif-sur-Yvette, France (cores 9CASQ and 1Comp). The conventional ages were then calibrated using the CALIB 7.1 online calibration software (Stuiver *et al.* 2017) and the MARINE13 calibration curve (Reimer *et al*. 2013) with a regional reservoir correction ΔR of 220 ± 20 years (Coulthard *et al*. 2010). Of the 6 samples that were analyzed, only the results of sample ECHo 2559 could not be validated, since only 1 µg of carbon was detected.

Results

Sea floor morphology and stratigraphic framework

184 *Subbottom profiles*. The acoustic subbottom profiles (3.5 kHz) from the sampling location of core 9CASQ show high amplitude parallel acoustic reflections at the middle of the core (between 362 to 125 cm) where a turbidite and alternating mud and IRD layers are observed. These units are topped by an acoustically transparent unit associated with postglacial hemipelagic sediments (Fig. 3A). However, given the loss of the signal at the base of the core (between 552 and 362 cm), the seismic profile in Fig. 3A does not reflect the stratigraphy at the base. The seismic profile of core 77PC is modified from Campbell & Bennett (2014) and is characterized by high amplitude parallel reflections in the basal part of the core and transparent acoustic facies associated with the hemipelagic sediments in the upper part of the core (Fig. 3B; Campbell & Bennett 2014). For core 1Comp, the sequence is characterized by a high amplitude reflection that can be associated with the debrite observed at the base of the core, whereas the uppermost acoustically transparent unit is interpreted as postglacial hemipelagic sediments (Fig. 4). The available data within the cross-shelf trough, including the airgun profile (Fig. S1), do not show any seismic unit that could be interpreted as a grounding-zone wedge (GZW).

Swath bathymetry. Glaciogenic landforms associated with the presence of the LIS and/or icebergs drifting offshore were identified and mapped using the swath bathymetry imagery. Linear, curvilinear, and almost circular depressions with a general N-S orientation, occur at the eastern end of the trough. These are interpreted as the product of iceberg keels eroding the seafloor (Figs 5A, B, S2; Brouard & Lajeunesse 2019A). Sets of other erosional landforms aligned parallel to the trough axis (W-E) are also observed in the Home Bay Trough. Three distinct landforms can be interpreted within the trough: 1) large ridges that are similar in terms of width (km) to subglacial medial moraines in other Baffin Island troughs (Brouard &

Lajeunesse 2017); 2) smaller-scale longitudinal ridges that have morphologies similar to mega-scale glacial lineations (MSGL; Clark 1993; Stokes & Clark 2002); and 3) curvilinear depressions that are interpreted as iceberg scours (Fig. 5B). The seaward end of the cross-shelf trough is characterized by a series of parallel gullies, some of which extending downslope to form turbidity channels with distinctive levees (Figs. 5A, S2, S6). Such channels are generally eroded by underflows or currents transporting sediment downslope and have been reported on other high-latitude shelves and in fiords (Syvitski & Shaw 1995; Syvitski *et al*. 2012; Dowdeswell & Vásquez 2013; Brouard & Lajeunesse 2019B).

Lithofacies

The classification of these facies was determined from CAT-scan images, physical and magnetic properties, as well as previous studies from Baffin Bay (Andrews 1985; Tripsanas & Piper 2008; Ó Cofaigh *et al*. 2013; Simon *et al*. 2012; Jackson *et al*. 2017; Jenner *et al*. 2018). Photography and CAT-scan images reveal a highly variable lithology across the cores (Figs. 2, 7). Overall, seven lithofacies were identified in the two cores from the TMF (1Comp and 9CASQ; Figs. 6, 7). Lithofacies 1 (LF1) is defined as a massive, matrix-supported diamicton facies with very dense, black, and coarse-grained sediment. It is mixed with a fine-grained matrix and has a sharp upper contact. This facies contains a concentration of granules, pebbles, and cobbles, which are angular to sub-rounded in shape. Lithofacies 2 (LF2) is defined as a laminated dark gray to dark grayish-brown silty mud, rich in IRD, with an unrhythmic succession of stratified pebbly mud. The concentrated pebbles often deform the laminae and contacts range from diffuse to sharp (Fig. 2). Lithofacies 3 (LF3) is defined as dense, very dark gray silts and sands with clasts. Facies LF3 is composed of coarse-based fining upward laminated mud with normal grading (Fig. 8). The upper contact of this layer is also visible, as shown by the contrast between the finer sediment and the background sediments immediately above (Figs. 6, 8; St-Onge *et al*. 2004; Bourget *et al*. 2011; Pouderoux *et al*. 2012). Lithofacies 4 (LF4) is defined as a laminated dark grayish-brown rhythmic succession of clay and silt laminae. The laminae and contacts range from diffuse to very sharp and do not contain IRD or bioturbation. Lithofacies 5 (LF5) is defined as a massive homogenous dark grayish-brown silty mud with IRD. No apparent structures are observed. The distribution of pebbles within LF5 ranges from dispersed to concentrated and the contacts range from diffuse to gradual. Lithofacies 6 (LF6) is defined as a carbonate-rich light olive brown sandy and pebbly mud with IRD. Finally, lithofacies 7 (LF7) is defined as a massive and homogenous bioturbated grayish to brownish mud without IRD. Apart from traces of bioturbation such as well-defined burrows, no apparent structures are observed in this lithofacies (Fig. 2).

Interpretation of lithofacies

LF1 exhibit characteristics (massive, matrix-supported diamicton facies) that are similar to GDFs triggered near an ice-sheet margin and that have been described at the margin of other deglaciated shelves (King *et al*. 1998; Ó Cofaigh *et al*. 2013). The IRD rich silty mud of the LF2 facies suggests that it was probably deposited during episodes of warming leading to sea-ice cover break-ups which enables icebergs to drift along currents (Dowdeswell *et al*. 2000). However, the laminated character of LF2 also suggests other possible processes for deposition; the laminations could result from turbidity current activity and/or turbid meltwater plumes originating from glacial ice on the shelf. These laminations would reflect the evolution in time of meltwater discharge from proximal tidewater glaciers (Cowan & Powell 1990; Andrews *et al*. 1991;

Dowdeswell & Cromack 1991; Jennings 1993; Dowdeswell *et al*. 2000; Jenner *et al*. 2018). This assumption is supported by the fact that during winter or a long phase of climate cooling, ice covers all of Baffin Bay and traps icebergs, suppressing their drift offshore. In this case, meltwater discharge will be dominant if there is no delivery of coarser debris. Cowan et al. (1997) suggested the opposite and proposed punctuated IRD deposition occurs in winter and turbid meltwater deposition, dominated by turbidity currents and suspension deposits, occurs in summer. One way or the other, the fine-grained laminated glaciomarine sediments are usually not regarded as typical of icebergs-dominated areas, but sometimes they can vary rhythmically with IRD and rapidly deposited layers (Domack 1990; Dowdeswell *et al.* 2000). Overall, both processes (IRD and turbidity current deposition) probably reflect punctuated IRD deposition during winters and turbid meltwater deposition, dominated by turbidity currents and suspension deposits, during summers (Cowan *et al.* 1997). A similar layer in core 9CASQ represents a glaciomarine environment. Suspension deposit sedimentation during periods of continuous sea-ice cover probably generated the mud of this unit. The hypothesis of multiyear sea-ice cover of the core sites is reinforced by the scarcity of foraminifera, as continuous sea-ice cover suppresses biological activity (Syvitski 1989; Dowdeswell *et al.* 2000).

The coarse-grained laminated mud at the base of LF3 and its normal grading is suggestive of a silty and sandy turbidite. Core 9CASQ was collected at 1220 m water depth and contains such LF3 layer (Figs. 6, 8). As the Baffin Island Current (BIC) is particularly strong at 1000–1200 water depth on the Baffin Bay Slope (Dunlap & Tang 2006) and can trigger low density muddy turbidity currents on the Baffin Bay Slope. LF3 facies could be interpreted as a turbidite resulting from bottom current activity (Dunlap & Tang 2006; Roger *et al*. 2013; Jenner *et al*. 2018).

Rhythmic succession of clay and silt laminae with diffuse contacts and without IRD and bioturbation in LF4 can be deposited through various processes in northern environments, such as the deposition by meltwater plumes (Hesse *et al*. 1997), as mud turbidites seaward of glacial troughs (Roger *et al*. 2013) and as subglacial outbursts of turbid meltwaters (Lucchi *et al*. 2013). In cores 9CASQ and 1Comp, this facies mostly overlies a debrite or turbidite. We therefore associate it with muddy density flows and meltwater plumes emanating from glacial discharge during ice retreat.

The massive and homogenous character of LF5 mud indicates a low-energy environment that probably reflects the absence of glacial activity near the core site. The frequent IRD of LF5 relate to drifting icebergs and suggests that a significant portion of Home Bay was ice-free at this time.

The carbonate-rich sandy and pebbly mud with IRD of LF6 is similar to ice-rafted, carbonate-rich sediments observed all around Baffin Bay (Andrews *et al*. 1998, 2009; Jackson *et al*. 2017). These layers, named Baffin Bay Detrital Carbonate layers (e.g. Andrews *et al.* 1998; Simon *et al.* 2014) are associated with episodes of high iceberg activity originating from NW Baffin Bay (Aksu & Piper 1987) and have been dated to 10.5-12 (BBDC0) and 13.7-15 cal. ka BP (BBDC1; Simon *et al*. 2014). Aksu & Piper (1987) suggested that northwestern Baffin Bay, Devon and Ellesmere Islands and northwestern Greenland are the source of the lower Palaeozoic limestones and dolomites observed in sediments transported as IRD to southern Baffin Bay. In contrast with the previous facies, which were rich in ice rafted debris (IRDs), LF7 contains massive and homogenous bioturbated mud without IRD in the uppermost part of the core and reflects hemipelagic sedimentation in a postglacial environment similarly to other uppermost parts of cores recovered in Baffin Bay (e.g. Dowdeswell *et al*. 2008; Ó Cofaigh *et al*. 2013).

Physical, stratigraphic and magnetic properties

Core 77PC. Core 77PC is used here as a chronostratigraphic reference core; Jenner *et al*. (2018) provided a detailed description of the core together with original ages. Overall, this core is composed of laminated and bioturbated mud, wavy silty laminae and detrital carbonate layers but contains no rapidly deposited layers. The grain size results show relatively fine material with an average of ~5 µm in the entire core (Fig. 6A). Between 161 and 117 cm, a sharp increase in the density and MAD values is observed, as well as a decrease in the inclination and NRM values. Aside from this interval, the NRM values are relatively constant (~ 0.02 A m^{-1}), but peaks are seen in the ARM, IRM, and SIRM profiles between 310 and 270 cm, as well as between 470 and 450 cm (Fig. 6A). Nonetheless, the MAD values are lower than 5° in the entire core, indicating high quality palaeomagnetic data except for a few intervals.

The ChRM was determined after using a 5 mT demagnetization steps between 10 and 60 mT. The ChRM fluctuates around the expected inclination value for the coring site that was calculated according to the geocentric axial dipole model (I_{GAD}), denoting a well-recorded palaeomagnetic signal (Fig. 6A; Stoner & St-Onge 2007). The downcore MAD values are generally lower than 2°, indicative of a very well-defined ChRM. The MDF_{NRM} values fluctuate between 20 and 40 mT throughout the core with an average of 35 mT. Such an average indicates the presence of low coercivity minerals such as magnetite, except for a few very thin intervals where MDF values close to 50 mT are observed.

Core 1Comp. The correlation between the density measured on the piston and the trigger weight core 01 suggests that approximately 30 cm of sediment was lost during the piston coring. This missing sediment was taken into account when constructing the composite profile (Fig. S3).

The physical and magnetic properties allow the identification of 5 distinct stratigraphic units (Figs. 6B, 7). The base of the core extends from 381 to 175 cm and is characterized by a thick and poorly sorted layer with high density values. This layer showing the LF1 facies is absent in 9CASQ and core 77PC.

Overlying LF1, LF4 layer extends from 175 to 161 cm, has low magnetic susceptibility, good sorting and a mean grain size ~3 µm. The coarse material from LF5 (161-129 cm) reflects the high values of magnetic susceptibility that peaks at approximately 400×10^{-5} SI, which is due to the presence of pebbles containing a high concentration of ferrimagnetic minerals. Unit 5 (LF5) extends from 161 to 129 cm.

Over LF4 lies a layer (117-65 cm) showing distinct peaks in Ca/Sr ratio (Fig. 6B) reflecting a high carbonate content. The Ca/Sr ratio averages approximately 100 throughout the core 1Comp, but reaches 750 at 85 cm. In addition, between 117 and 65 cm, the MAD values reach 30° at 100 cm, as well as a decrease in inclination and remanence values (NRM, ARM, IRM, SIRM; Fig. 6B). These results attest to the presence of detrital carbonate probably associated to BBDC events (Fig. 6B; e.g. Balsam *et al.* 1999; Hodell *et al.* 2008; Channell *et al.* 2012; Winsor *et al.* 2012; Simon *et al.* 2014, 2016; Jackson *et al.* 2017). LF7 tops the core from 65 to 0, but also from 129 to 117 cm.

The NRM, ARM, IRM and SIRM values are variable throughout this core (Fig. 6B). Inclination values in this core also generally fluctuate around the expected values of the GAD with MAD values below 5°, indicating high quality palaeomagnetic data (Stoner & St-Onge 2007; Tauxe 2010). Shallower inclinations and much higher MAD values are observed between

381-175 (LF1), 161-115 and 117-65 cm (BBDC). In LF1, the alternating negative and positive inclination values denote the presence of clasts (Fig. 6B). The MDF_{NRM} values fluctuate between 30 and 55 mT (aside from the debris flow deposit, which shows low values and have an average of approximately 45 mT (Fig. 6B); these values indicate the presence of low coercivity minerals, such as magnetite, and a contribution from higher coercivity minerals (Tauxe & Wu 1990; Stoner *et al*. 2000).

Core 9CASQ. Core 9CASQ is characterized by 6 lithofacies (Figs. 6C, 7). LF2 facies forms the lower part of the core (550-362 cm) and is characterized by a succession of stratified pebbly mud with frequently deformed, diffuse to sharp, parallel laminations and some IRDs (Fig. 6C). The lowermost part of LF2 reveal small peaks in mean grain size and in sorting that could be related to small turbidity current activity. Over LF2, a coarser layer of LF3 (362-340 cm) shows high density and CT number, and magnetic susceptibility values of up to ~400 × 10^{-5} SI (Fig. 6C). Over LF3, two distinct intervals of the LF4 facies (241-211 and 340-305 cm) consisting of a rhythmic succession of clay and silt laminae alternate with homogeneous muds without IRDs (LF7; 305-275 and 125-0 cm) and layers with carbonate peaks (LF6; 211-125 cm), which can be related to BBDC.

The grain size distribution shows relatively constant variations throughout the core, ranging from fine clay to coarse silt with an average of 4 µm, except in three distinct layers with increased average values, which correspond respectively to LF3 (362-340 cm; Figs. 6C, 7, 8) and two thin layers at the base of LF2 (544-536 and 533-523 cm; Fig. 6C). These three layers are also less sorted than the rest of the core and show a normal grading typical of turbidites (Fig. 8; e.g. St-Onge *et al*. 2004; Bourget *et al*. 2011; Pouderoux *et al*. 2012). LF3 is characterized by low basal palaeomagnetic inclinations and high MAD values (Figs. 6C, 8; St-Onge *et al*. 2004; Philippe 2019).

The ChRM inclination along the core generally fluctuates around the expected inclination values (I_{GAD}) and MAD values are lower than 2°, indicative of very well-defined palaeomagnetic data, except for the detrital carbonate and turbidite layers (LF6 and LF3), which have low inclination (Fig. 8) and high MAD values. Aside from LF6, the MDF_{NRM} values range between 20 and 40 mT with an average of 30 mT, which is indicative of low coercivity minerals such as magnetite (Fig. 6C). The sharp increase in MDF values in the detrital carbonate layer indicates a lower concentration of magnetite and a higher concentration of coercivity minerals in this layer (Simon *et al*. 2012).

Magnetic properties

Day plots (Fig. 9B) indicate that most of the sediments of the three cores are composed of magnetic grains in the pseudo single domain (PSD) range with only few samples from cores 1Comp and 9CASQ falling in the multi-domain range (MD). The samples in the MD range reflect the coarser grains observed in the rapidly deposited layers (e.g. turbidite and debrite). The magnetic k_{ARM}/k diagram (King *et al*. 1983) for the three cores indicates that the magnetic grain size is relatively fine and under 5 µm. The absolute magnetic grain size values should be interpreted with caution because these empirical relationships were derived from synthetic magnetic grains. However, taken together with the results from the Day plot, these values suggest an optimal PSD range for palaeomagnetic reconstructions (e.g. Tauxe 1993).

The shape of the hysteresis curves of the discrete samples from the three cores are typical of low coercivity ferrimagnetic minerals such as magnetite (Fig. 9A; Tauxe *et al*. 1996; Dunlop

& Özdemir 1997). In addition, the magnetic mineralogy-dependent ratio IRM/SIRM (Pseudo S-ratio) is useful for estimating changes in magnetic mineralogy, with values close to 1 indicating a low-coercivity ferrimagnetic mineralogy (e.g. magnetite; St-Onge *et al*., 2003). The S-ratio in cores 77PC, 1Comp and 9CASQ, with mean values of 0.992, 0.988 and 0.987, respectively, suggest that low coercivity minerals, such as magnetite, are the dominant magnetic carriers. Moreover, the MDF_{NRM} values range from 25 to 40 mT, which also suggest the presence of magnetite and/or titanomagnetite throughout most of the 3 cores (Fig. 6). On the other hand, sediments of LF1 and LF6 in core 1Comp are characterized by lower MDF values that indicate the occurrence of coarser magnetic grains, as seen in the Day plot (Fig. 9B) and in the physical grain size data (Fig. 9C). Finally, changes in the NRM, ARM, IRM, and SIRM values vary by less than an order of magnitude.

Relative palaeointensity (RPI) determination and chronostratigraphy

The magnetic properties of the cores indicate that the NRM of most of the sediments, apart from RDL, is characterized by a strong, stable, single component magnetization carried by PSD magnetite grains, thus fulfilling the established criteria to derive a reliable RPI proxy (e.g. Levi & Banerjee 1976; Tauxe 1993; Stoner & St-Onge 2007; Yamazaki *et al*. 2013). Moreover, the comparison between ARM and IRM as normalizers seems to activate the same magnetic assemblages (Levi & Banerjee 1976) and the differences between the ARM and IRM as normalizers also suggest that ARM has a slightly better R^2 then IRM (Figs. S4, S5). The comparison of the normalized remanence with its normalizer among the 3 cores indicates that NRM/ARM is not correlated with the ARM when rapidly deposited layers are excluded (Fig. S4). Conversely, the same comparison indicates a correlation for RDL (e.g. debrite and turbidite; LF1 and LF3) and detrital carbonates (DC) layers (LF6) with R^2 values of 0.37 and 0.40, respectively (Fig. S4). Based on these results, ARM has been selected as the best normalizer. Detrital carbonate layers were then excluded from palaeomagnetic reconstructions, but RDL values, even if they do not yield appropriate results, have been retained in the figures to give the reader a glimpse of their age-depth relationship.

Discussion

RDL layers: debrite and turbidite

Glaciogenic debris flow deposits are major components of TMFs (Fig. 10; Laberg & Vorren 1995; King *et al*. 1998; Vorren *et al*. 1998; Nygard *et al*. 2002). In Home Bay, LF1 is characterized by a massive, matrix-supported diamicton facies with clasts, the highest MAD values, and low values of palaeomagnetic inclinations (Fig. 6B). This combination of parameters clearly indicates that a debrite was recorded. Magnetic properties of sediments can be a source of significant information for the interpretation of sedimentary products. In fact, turbidites, debrites and detrital carbonate layers generate higher MAD values (>5°) and highly variable inclinations which move away from the expected values. If the inclination is highly variable and very low such as in LF1 or LF3 it has no geomagnetic meaning, but it indicates the presence of rapidly deposited layers (Figs. 6B, C, 8).

Both physical and magnetic profiles of the 9CASQ highlight the presence of a turbidite (LF3) in the most distal part of Home Bay TMF (Fig. 5A). The turbidite contrasts sharply with hemipelagic muds and IRD layers associated with the continuous “background” sedimentation (Figs. 6B, 7). The presence of a debrite and a turbidite attests to the sensitivity of Home Bay TMF for capturing mass wasting events on the shelf edge. The glacial debris flow reflect the

437 presence of nearby glacial ice alike LGM sedimentary processes of other glaciated continental
438 slopes: large debris flows were generated and accumulated down the slope on the trough-mouth
439 fans when the local ice sheets reached the shelf break (Fig. 10; e.g. Laberg & Vorren 1995;
440 Laberg *et al.* 1995; Dowdeswell *et al.* 1996; Laberg & Vorren 1996a; Vorren & Laberg 1997;
441 King *et al.* 1998; Dowdeswell & Siegert 1999; Batchelor *et al.* 2014, 2015). Subbottom profiles
442 over the sampling location of core 1Comp (Figs. 1B, 4, S6) reveal that the acoustic facies
443 associated with the debris flow extends laterally to form a series of stacked debris flow deposits
444 which accumulated inside this TMF (Figs. 4, 10). Subglacial landforms such as MSGLs and
445 deeply-incised iceberg ploughmarks that are oriented in the trough axis also suggest that glacial
446 ice extended near the shelf edge to later retreat while calving deep-keeled icebergs. Icebergs
447 flowing along the BIC most likely produced iceberg ploughmarks scars that are oriented N-S.
448 However modern-day drafts of icebergs flowing through Baffin Bay rarely exceed 300 m (Praeg
449 *et al.* 2006), indicating that they cannot account for the deep keel scours that occur below 300 m
450 within the trough (Praeg *et al.* 2006). This suggests ploughmarks are not modern and that they are
451 most likely resulting from deep glacial ice grounding in Baffin Bay. The orientation of the
452 ploughmarks within the trough suggests that the icebergs responsible for the deep keel erosion
453 were originating from within the trough. The ice flow landforms (MSGLs) within the trough can
454 be interpreted as a signature of ice stream activity while the several channels on the TMF have
455 probably been eroded by sediment-rich meltwaters from nearby glacial ice (Fig. 5B; Ottesen *et*
456 *al*. 2005; Montelli *et al*. 2017). Such sediments can be transported by ice streams and be advected
457 towards the slope where they can take the shape of debris flows (e.g. Laberg & Vorren 1995;
458 Lasabuda *et al*. 2018) and turbidity currents. The several canyons and gullies could have formed
459 routes for remobilizing sediments from the upper slope to their accumulation site in the basin
460 (Figs. 5A, S6; e.g. Lasabuda *et al*. 2018).

Late Quaternary Baffin Bay chronostratigraphy

While the geophysical data point towards the LIS extending near the shelf edge during the LGM, ages are needed to define whether the debrite or the turbidite are of LGM age. The 3 studied cores show similar relative palaeointensity (RPI) features that can be correlated on a regional and hemispheric scale. A combination of radiocarbon ages and palaeomagnetic tie points were used to determine the chronology of the cores. Therefore, the cores can produce a chronostratigraphic framework for the last 45 ka (Fig. 11).

A comparison between the cores and other RPI records from the Northern Hemisphere indicate that the geomagnetic origin of the signal in the 0–45 ka interval for cores 77PC, 9CASQ and 1Comp is consistent with the available radiocarbon ages (Fig. 11). Based on this comparison and the chronological model, we suggest that the debrite observed in core 1Comp was deposited before 15 cal. ka BP, while the turbidite (LF3) in 9CASQ was deposited at approximately 20 cal. ka BP. Subbottom profiles (3.5 kHz) from the coring site of core 1Comp illustrates that the core was collected on the side edge of a debris flow channel (Figs. 4, 5A, S6) in a thin, side section of the channel and therefore record the full sequence since the last debris flow (i.e. since 15 ka BP). Without discarding the possibility of an earthquake in the Baffin Bay area at this time, the turbidite recorded in core 9CASQ was dated from the Last Glacial episode (~20 ka BP) and could have been triggered by the presence of the LIS margin on the continental shelf. Previous work showed that large volumes of turbidites along ice margins are related to subglacial outbursts and can be used as a proxy to determine a glaciomarine source (Dowdeswell *et al*. 1998; Hesse *et al*. 1999; Toucanne *et al*. 2012). There is still no general agreement in regards to which sedimentary structures can be used to distinguish fine-grained turbidites from contourites (Hollister 1967;

Hollister & Heezen 1972; Piper 1972). Some authors contend that fine turbidite deposits such as LF3 in core 9CASQ can be differentiated from those of contourites based on certain characteristics: the absence of widespread burrowing, bioturbation, a lack of a vertical sequence of structures (Lovell & Stow 1981; Stow & Piper 1984) and traction sedimentary structures (Carter *et al*. 1996; Wynn & Stow 2002; Shanmugam 2006). These criteria are considered to be diagnostic of fine-grained turbidites rather than contourites: therefore, together with geophysical and sedimentological data, the graded sediment in LF3 is interpreted as a glaciogenic turbidite.

The occurrence of >15,000 years-old GDFs and turbidity current deposits on the Home Bay TMF together with glacial lineations clearly indicate that the LIS advanced near the shelf edge during the Last Glacial episode. According to several authors, the maximum extension of the LIS in the Home Bay area probably lasted up to ~14-12 cal. ka BP (Dyke *et al*. 2002; Margold *et al*. 2015). The chronostratigraphy obtained by a combination of palaeomagnetism and radiocarbon ages shows that debrites were being deposited in the Home Bay TMF until around 15 cal. ka BP, which approximately marks the beginning of the Bølling warm period (Deschamps *et al.* 2012). Hence, perennial temperatures and precipitation during post-LGM and pre-Bølling were cold and/or precipitations high enough to keep the ice margin near the shelf edge. This late retreat of the LIS margin offshore Home Bay is somehow similar to persistent glacial ice in southern regions (e.g. Des Moines lobe, James Bay lobe, and Great Lakes lobes; Dyke 2004) which only show significant retreat after 15 cal. ka BP. This pattern could point out to a similar response of the LIS to the Bølling warming over all its extent.

Conclusions

New geomorphological, stratigraphic and sediment core data coupled with the dating of glaciogenic debrite and turbidite allowed to reconstruct the activity of the LIS margin in the Home Bay trough and trough-mouth fan during the Last Glacial episode. The following results suggest that an ice margin extended near the shelf edge of Home Bay during the Last Glacial episode:

- Seven lithofacies within the cores depict a full glacial-deglacial-postglacial sedimentary sequence: i) rapidly deposited layers such as a debrite and a turbidite generated in a glacial environment; ii) sediments from meltwater plumes, turbidity currents and possibly bottom currents generated in an ice-proximal environment; iii) ice-rafted debris deposited since the last deglaciation; and iv) postglacial hemipelagic sediments.
- Chronostratigraphy from the core 9CASQ indicate that the turbidite observed was probably transported along the slope of Home Bay trough-mouth fan during the LGM.
- High-resolution swath bathymetry data allowed the identification of subglacial landforms related to ice-stream activity near the shelf edge. The subglacial landforms, such as mega-scale glacial lineations (MSGLs), together with the age of the debrite and the turbidite, indicates that glacial processes have eroded and molded the shelf during and since the LGM.

Finally, this paper outlines the usefulness of combining palaeomagnetic measurements with radiocarbon dating for establish a reliable chronostratigraphy in an environment where calcium carbonate dissolution challenges the use of foraminifera for dating.

Index of abbreviations: TMF: trough-mouth fan; GDF : glaciogenic debris flows; LIS : Laurentide Ice Sheet; IIS: Innuitian Ice Sheet; GIS : Greenland Ice Sheet; LGM: Last Glacial Maximum; BIC: Baffin Island Current; 9CASQ: AMD16-LGM-09; 1Comp: AMD0217-01PC and AMD0217-01TWC; 77PC: HU2013-029-0077; LF1 to LF7: Lithofacies 1 to 7; RDL: rapidly deposited layer; BBDC: Baffin Bay detrital carbonates; GZW: grounding-zone wedge; MSGL: mega-scale glacial lineation; MSCL: Multi Sensor Core Logger; XRF: X-ray fluorescence. Palaeomagnetic parameters: k_{LF}: magnetic susceptibility; NRM: natural remanent magnetization; ARM: anhysteretic remanent magnetization; IRM : isothermal remanent magnetization; SIRM: saturation isothermal magnetization; ChRM: characteristic remanent magnetization; MAD: maximum angular deviation; MDF: median destructive field;

I_{GAD}: axial dipole model; PSD: pseudo single domain; SD: single domain; PSV: palaeomagnetic secular variation; RPI: relative palaeointensity; Ms: saturation magnetization; Hc: coercive force; Mrs: saturation remanence; Hcr: coercivity of remanence; AMS: accelerator mass spectrometry; AGM: alternating gradient force magnetometer; AF: alternating field; DC: direct current

Acknowledgements. —We thank Calvin Campbell from the Geological Survey of Canada for access to core 77PC and its radiocarbon ages. We also sincerely thank the captains, officers, crew and scientists on board of CCGS Amundsen for the recovery of the cores used in this study. We also thank Quentin Beauvais (ISMER) and Marie-Pier St-Onge (ISMER) for their technical support and advice in the laboratory as well as Jean-Carlos Montero-Serrano (ISMER) for his help collecting several of the cores studied. This research was funded by the ArcticNet Network of Centres of Excellence of Canada and by the Natural Sciences and Engineering Research Council of Canada (NSERC) through Discovery grants to G.S. and P.L. Finally, we are thankful to the editor Jan A. Piotrowski, Calvin Campbell, Kimberley Jenner and Amando Lasabuda for providing constructive comments that helped to improve the manuscript. Author contributions: Y.L. performed the laboratory measurements, processed and analysed the data, wrote the various versions of the manuscript and made the figures; G.S. designed and supervised all the measurements and writing; P.L was responsible for the 2016 and 2017 CCGS Amundsen expeditions and supervised the geophysical aspects of the manuscript and writing. P.A.D. contributed to the geophysical data processing and analyses as well as preparation of related figures. E.B. contributed to the interpretation of the geomorphological data and glacial dynamics in Baffin Bay and to the final version of the manuscript. The other authors contributed to all the various versions of the manuscript.

References

Aksu, A. E. & Piper, D. J. W. 1987: Late Quaternary sedimentation in Baffin Bay. *Canadian Journal of Earth Sciences 24*, 1833–1846.

Andrews, J. T. 1985: Quaternary environments : Eastern Canadian Arctic, Baffin Bay and Western Greenland. 774 pp. Allen & Unwin, Boston.

Andrews, J. T., Kirby, M., Jennings, A. & Barber, D. 1998: Late Quaternary stratigraphy, chronology, and depositional processes on the slope of SE Baffin Island, detrital carbonate and Heinrich events: Implications for onshore glacial history. *Géographie physique et Quaternaire 52*, 91–105.

Andrews, J. T. & Jennings, A. E. 1990: Geomagnetic secular variations (inclination) of high-latitude fjord cores—Eastern Canadian Arctic. *Polar Research 8*, 245–259.

Andrews, J. T, Jennings, A. E., MacLean, B., Mudie, P. J., Praeg, D. & Vilks, G. 1991: The surficial geology of the Canadian eastern Arctic and Polar continental shelves. *Continental Shelf Research 11*, 791–819.

Andrews, J. T., Kirby, M., Jennings, A. E. & Barber, D. C. 2009: Late Quaternary stratigraphy, chronology, and depositional processes on the slope of S. E. Baffin Island, detrital carbonate and Heinrich events: implications for onshore glacial history. *Géographie physique et Quaternaire 52*, 91–105.

Balsam, W. L., Deaton, B. C. & Damuth, J. E. 1999: Evaluating optical lightness as a proxy for carbonate content in marine sediment cores. *Marine Geology 161*, 141–153.

Barletta, F., St-Onge, G., Channell, J. E. T., Rochon, A., Polyak, L. & Darby, D. 2008: High-resolution palaeomagnetic secular variation and relative palaeointensity records from the western Canadian Arctic: implication for Holocene stratigraphy and geomagnetic field behaviour. *Canadian Journal of Earth Sciences 45*, 1265–1281.

Barletta, F., St-Onge, G., Channell, J. E. T. & Rochon, A. 2010: Dating of Holocene western Canadian Arctic sediments by matching palaeomagnetic secular variation to a geomagnetic field model. *Quaternary Science Reviews 29*, 2315–2324.

Batchelor, C. L. & Dowdeswell, J. A. 2014: The physiography of High Arctic cross-shelf troughs. *Quaternary Science Reviews* 92, 68–96.

Batchelor, C. L. & Dowdeswell, J. A. 2015: Ice-sheet grounding-zone wedges (GZWs) on high-latitude continental margins. *Marine Geology 363*, 65–92.

Bourget, J., Zaragosi, S., Ellouz-Zimmermann, N., Mouchot, N., Garlan, T., Schneider, J.-L., Valentine, L. & Lallemant, S. 2011: Turbidite system architecture and sedimentary processes along topographically complex slopes: the Makran convergent margin. *Sedimentology 58*, 376–406.

Briner, J. P., Miller, G.H., Davis, P.T. & Finkel, R.C. 2005: Cosmogenic exposure dating in arctic glacial landscapes: implications for the glacial history of northeastern Baffin Island, Arctic Canada. *Canadian Journal of Earth Sciences* 42, 67-84.

Briner, J. P., Michelutti, N., Francis, D. R., Miller, G. H., Axford, Y., Wooller, M. J. & Wolfe, A. P. 2006: A multi-proxy lacustrine record of Holocene climate change on northeastern Baffin Island, Arctic Canada. *Quaternary Research 65*, 431–442.

Briner, J. P., Miller, G.H., Davis, P.T. & Finkel, R.C. 2006: Cosmogenic radionuclides from fiord landscapes support differential erosion by overriding ice sheets. *Geological Society of America Bulletin* 118, 406-420.

Brouard, E. & Lajeunesse, P. 2017: Maximum extent and decay of the Laurentide Ice Sheet in Western Baffin Bay during the last glacial episode. *Scientific Reports 7*.

Brouard, E. & Lajeunesse, P. 2019A: Glacial to postglacial submarine landform assemblages in fiords of northeastern Baffin Island. *Geomorphology* 330, 40–56.

Brouard, E. & Lajeunesse, P. 2019B: Submarine geomorphology of the northeastern Baffin Island fiords and cross-shelf troughs. *Journal of Maps* 15, 662-676.

Campbell, D. C. 2014: CCGS Hudson Expedition 2013-029. Geological hazard assessment of Baffin Bay and biodiversity assessment of Hatton Basin. *Open file 7594*, 124 pp. Geological survey of Canada.

Campbell, D. C. & Bennett, J. R. 2014: Preliminary results from recent investigations of marine geological hazards in Baffin Bay, Nunavut and Greenland. *Summary of Activities 2013*, 121–128. Canada-Nunavut Geoscience Office.

Carter, R. M., Carter, L. & McCave, I. N. 1996: Current controlled sediment deposition from the shelf to the deep ocean: the Cenozoic evolution of circulation through the SW Pacific gateway. *Geologische Rundschau 85*, 438–451.

Channell, J. E. T., Hodell, D. A., Romero, O., Hillaire-Marcel, C., de Vernal, A., Stoner, J. S., Mazaud, A. & Röhl, U. 2012: A 750-kyr detrital-layer stratigraphy for the North Atlantic (IODP Sites U1302—U1303, Orphan Knoll, Labrador Sea). *Earth and Planetary Science Letters 317*, 218–230.

Clark, C. D. 1993: Mega-scale glacial lineations and cross-cutting ice-flow landforms. *Earth Surface Processes and Landforms* 18, 1–29.

Coulthard, R. D., Furze, M. F. A., Pieńkowski, A. J., Nixon, F. C. & England, J. H. 2010: New marine ΔR values for Arctic Canada. *Quaternary Geochronology 5*, 419–434.

Cowan, E. A. & Powell, R. D. 1990: Suspended sediment transport and deposition of cyclically interlaminated sediment in a temperate glacial fjord, Alaska, USA. *Geological Society, London, Special Publications 53*, 75–89.

Cowan, E. A., Cai, J., Powell, R. D., Clark, J. D. & Pitcher, J. N. 1997: Temperate glacimarine varves: an example from Disenchantment Bay, southern Alaska. *Journal of Sedimentary Research 67*, 536–549.

Day, R., Fuller, M. & Schmidt, V. A. 1977: Hysteresis properties of titanomagnetites: grain-size and compositional dependence. *Physics of the Earth and Planetary Interiors 13*, 260–267.

De Blasio, F. V., Elverhøi, A., Issler, D., Harbitz, C. B., Bryn, P. & Lien, R. 2004: Flow models of natural debris flows originating from overconsolidated clay materials. *Marine Geology 213*, 439–455.

Deschamps, P., Durand, N., Bard, E., Hamelin, B., Camoin, G., Thomas, A. L, Yokoyama, Y. 2012: Ice-sheet collapse and sea-level rise at the Bølling warming 14,600 years ago. *Nature* 483, 559-564.

de Vernal, A., Bilodeau, G., Hillaire-Marcel, C. & Kassou, N. 1992 : Quantitative assessment of carbonate dissolution in marine sediments from foraminifer linings vs. shell ratios: Davis Strait, northwest North Atlantic. *Geology* 20, 527–530.

de Vernal, A., Hillaire-Marcel, C., Aksu, A. E. & Mudie, P. J. 1987: Palynostratigraphy and chronostratigraphy of Baffin Bay deep sea cores: climatostratigraphic implications. *Palaeogeography, Palaeoclimatology, Palaeoecology 61*, 97–105.

Domack, E. W. 1990: Laminated terrigenous sediments from the Antarctic Peninsula: the role of subglacial and marine processes. *Geological Society, London, Special Publications 53*, 91–103.

Dowdeswell, J. A. & Cromack, M. 1991: Behavior of a glacier-derived suspended sediment plume in a small Arctic inlet. *The Journal of Geology 99*, 111–123.

Dowdeswell, J. A., Kenyon, N. H., Elverhøi, A., Laberg, J. S., Hollender, F., Mienert, J. & Siegert, M. J. 1996: Large-scale sedimentation on the glacier-influenced polar North Atlantic Margins: Long-range side-scan sonar evidence. *Geophysical Research Letters* 23, 3535–3538.

Dowdeswell, J. A., Elverhfi, A. & Spielhagen, R. 1998: Glacimarine sedimentary processes and facies on the polar North Atlantic margins. *Quaternary Science Reviews 17*, 243–272.

Dowdeswell, J. A. & Siegert, M. J. 1999: Ice-sheet numerical modeling and marine geophysical measurements of glacier-derived sedimentation on the Eurasian Arctic continental margins. *Geological Society of America Bulletin* 111, 1080–1097.

Dowdeswell, J. A., Whittington, R. J., Jennings, A. E., Andrews, J. T., Mackensen, A. & Marienfeld, P. 2000: An origin for laminated glacimarine sediments through sea-ice build-up and suppressed iceberg rafting. *Sedimentology 47*, 557–576.

Dowdeswell, J. A., Cofaigh, C. Ó., Noormets, R., Larter, R. D., Hillenbrand, C.-D., Benetti, S., Evans, J. & Pudsey, C. J. 2008: A major trough-mouth fan on the continental margin of the Bellingshausen Sea, West Antarctica: the Belgica Fan. *Marine Geology 252*, 129–140.

Dowdeswell, J.A. & Vásquez, M. 2013: Submarine landforms in the fjords of southern Chile: implications for glacimarine processes and sedimentation in a mild glacier-influenced environment. *Quaternary Science Reviews* 64, 1-19.

Dunlap, E. & Tang, C. C. L. 2006: Modelling the mean circulation of Baffin Bay. *Atmosphere-Ocean 44*, 99–109.

Dunlop, D. J. & Özdemir, Ö. 1997: Rock magnetism. Fundamental and Frontiers. 573 pp. Cambridge University Press, Cambridge.

Dyke, A. & Prest, V. 1987: Late Wisconsinan and Holocene history of the Laurentide ice sheet. *Géographie physique et Quaternaire 41*, 237–263.

Dyke, A. S., Andrews, J. T., Clark, P. U., England, J. H., Miller, G. H., Shaw, J. & Veillette, J. J. 2002: The Laurentide and Innuitian ice sheets during the last glacial maximum. *Quaternary Science Reviews 21*, 9–31.

Dyke, A. 2004: An outline of the deglaciation of North America with emphasis on central and northern Canada. *Developments in Quaternary Sciences 2,* 373-424.

Funder, S., Kjeldsen, K. K., Kjær, K. H. & Cofaigh, C. Ó. 2011: The Greenland Ice Sheet during the past 300,000 years: a review. *Developments in Quaternary Sciences 15*, 699–713.

Hesse, R., Khodabakhsh, S., Klaucke, I. & Ryan, W. B. F. 1997: Asymmetrical turbid surface-plume deposition near ice-outlets of the Pleistocene Laurentide ice sheet in the Labrador Sea. *Geo-Marine Letters 17*, 179–187.

Hesse, R., Klauck, I., Khodabakhsh, S. & Piper, D. 1999: Continental slope sedimentation adjacent to an ice margin. III. The upper Labrador Slope. *Marine Geology 155*, 249–276.

Hiscott, R. N., Aksu, A. E. & Nielsen, O. B. 1989: Provenance and dispersal patterns, Pliocene-Pleistocene section at site 645, Baffin Bay. *Proceedings of the Ocean Drilling Program, Scientific Results 105,* 31–52.

Hiscott, R. N. & Aksu, A. E. 1994: Submarine debris flows and continental slope evolution in front of Quaternary ice sheets, Baffin Bay, Canadian Arctic. *AAPG Bulletin 78*, 445–460.

Hodell, D. A., Channell, J. E. T., Curtis, J. H., Romero, O. E. & Röhl, U. 2008: Onset of "Hudson Strait" Heinrich events in the eastern North Atlantic at the end of the middle Pleistocene transition (~640 ka)? *Palaeoceanography 23*, PA4218.

Hollister, C. D. 1967: Sediment distribution and deep circulation in the western North Atlantic. PhD thesis. Columbia University.

Hollister C. D. & Heezen B. C. 1972: Geologic effects of ocean bottom currents. *In* Gordon A. L. (ed.): *Studies in Physical Oceanography—A Tribute to George Wust on his 80th Birthday,* 37–66, Gordon & Breach, New York.

Jackson, R., Carlson, A. E., Hillaire-Marcel, C., Wacker, L., Vogt, C. & Kucera, M. 2017: Asynchronous instability of the North American-Arctic and Greenland ice sheets during the last deglaciation. *Quaternary Science*

Reviews 164, 140–153.

Jakobsson, M., Mayer, L., Coakley, B., Dowdeswell, J. A., Forbes, S., Fridman, B., Hodnesdal, H, Noormets, R., Pedersen, R., Rebesco, M., Werner H. S. , Zarayskaya, Y., Accettella, D., Armstrong, A., Anderson, R. M., Bienhoff, P., Camerlenghi, A., Church, I., Edwards, MGardner, J. V., Hall, J. K., Hell, B., Hestvik, O., Kristoffersen, Y., Marcussen, C., Mohammad, R., Mosher, D., Nghiem, S. V., Pedrosa, M. T., Travaglini, P. G., Weatherall P. 2012: The international bathymetric chart of the Arctic Ocean (IBCAO) version 3.0. *Geophysical Research Letters 39*, L12609.

Jenner, K. A., Campbell, D. C. & Piper, D. J. W. 2018: Along-slope variations in sediment lithofacies and depositional processes since the Last Glacial Maximum on the northeast Baffin margin, Canada. *Marine Geology 405*, 92–107.

Jennings, A. 1993: The Quaternary history of Cumberland Sound, southeastern Baffin Island: the marine evidence. *Géographie physique et Quaternaire 47*, 21–42.

King, E. L., Haflidason, H. & Sejrup, H. P. 1998: Glacigenic debris flows on the North Sea Trough Mouth Fan during ice stream maxima. *Marine Geology 152*, 217–246.

King, J. W., Banerjee, S. K. & Marvin, J. 1983: A new rock-magnetic approach to selecting sediments for geomagnetic palaeointensity studies: Application to palaeointensity for the last 4000 years. *Journal of Geophysical Research: Solid Earth 88*, 5911–5921.

Laj, C., Kissel, C., Mazaud, A., Channell, J. E. T. & Beer, J. 2000: North Atlantic palaeointensity stack since 75ka (NAPIS—75) and the duration of the Laschamp event. *Philosophical Transactions of the Royal Society of London A: Mathematical, Physical and Engineering Sciences 358*, 1009–1025.

Laberg, J. S. & Vorren, T. O. 1995: Late Weichselian submarine debris flow deposits on the Bear Island Trough Mouth Fan. *Marine Geology 127*, 45–72.

Laberg, J. S. & Vorren, T. O. 1996a: The middle and late Pleistocence evolution and the Bear Island trough mouth fan. *Global and Planetary Change* 12, 309–330.

Lasabuda, A., Geissler, W. H., Laberg, J. S., Knutsen, S., Rydningen, T. A. & Berglar, K. 2018: Late Cenozoic erosion estimates for the northern Barents Sea: Quantifying glacial sediment input to the Arctic Ocean. *Geochemistry, Geophysics, Geosystems 19*, 4876-4903.

Ledu, D., Rochon, A., de Vernal, A. & St-Onge, G. 2008: Palynological evidence of Holocene climate change in the eastern Arctic: a possible shift in the Arctic oscillation at the millennial time scale. *Canadian Journal of Earth Sciences 45*, 1363–1375.

Levi, S. & Banerjee, S. K. 1976: On the possibility of obtaining relative palaeointensities from lake sediments. *Earth and Planetary Science Letters 29*, 219–226.

Li, G., Piper, D. J. W. & Calvin Campbell, D. 2011: The Quaternary Lancaster Sound trough-mouth fan, NW Baffin Bay. *Journal of Quaternary Science 26*, 511–522.

Li, G., Piper, D. J. W., Campbell, D. C. & Mosher, D. 2012: Turbidite deposition and the development of canyons through time on an intermittently glaciated continental margin: The Bonanza Canyon system, offshore eastern Canada. *Marine and Petroleum Geology 29*, 90–103.

Lovell, J. P. B. & Stow, D. A. V. 1981: Identification of ancient sandy contourites. *Geology 9*, 347–349.

Lucchi, R. G., Camerlenghi, A., Rebesco, M., Colmenero-Hidalgo, E., Sierro, F. J., Sagnotti, L., Urgeles, R., Melis, R., Morigi, C., Bárcena, M.-A., Giorgetti, G., Villa, G., Persico, D., Flores, J.-A., Rigual-Hernández, A. S. Pedrosa, M. T., Macri, P. & Caburlotto, A. 2013: Postglacial sedimentary processes on the Storfjorden and Kveithola trough mouth fans: Significance of extreme glacimarine sedimentation. *Global and Planetary Change 111*, 309–326.

Margold, M., Stokes, C. R. & Clark, C. D. 2015: Ice streams in the Laurentide Ice Sheet: Identification, characteristics and comparison to modern ice sheets. *Earth-Science Review 143*, 117–146.

Mazaud, A. 2005: User-friendly software for vector analysis of the magnetization of long sediment cores. *Geochemistry, Geophysics, Geosystems 6,* 3113-3115.

McKay, J. L., de Vernal, A., Hillaire-Marcel, C., Not, C., Polyak, L. & Darby, D. 2008: Holocene fluctuations in Arctic sea-ice cover: dinocyst-based reconstructions for the eastern Chukchi Sea. *Canadian Journal of Earth Sciences 45*, 1377–1397.

Meynadier, L., Valet, J.-P., Weeks, R., Shackleton, N. J. & Hagee, V. L. 1992: Relative geomagnetic intensity of the field during the last 140 ka. *Earth and Planetary Science Letters 114*, 39–57.

Montelli, A., Dowdeswell, J. A., Ottesen, D. & Johansen, S. E. 2017: Ice-sheet dynamics through the Quaternary on the mid-Norwegian continental margin inferred from 3D seismic data. *Marine and Petroleum Geology 80*, 228–242.

Nygard, A., Sejrup, H. P., Haflidason, H. & King, E. L. 2002: Geometry and genesis of glacigenic debris flows on the North Sea Fan: TOBI imagery and deep-tow boomer evidence. *Marine Geology 188*, 15–33.

Ó Cofaigh, C., Taylor, J., Dowdeswell, J. A. & Pudsey, C. J. 2003: Palaeo-ice streams, trough mouth fans and high-latitude continental slope sedimentation. *Boreas 32*, 37–55.

Ó Cofaigh, C, Andrews, J. T., Jennings, A. E., Dowdeswell, J. A., Hogan, K. A., Kilfeather, A. A. & Sheldon, C. 2013: Glacimarine lithofacies, provenance and depositional processes on a West Greenland trough-mouth fan. *Journal of Quaternary Science 28,* 13–26.

Ottesen, D., Dowdeswell, J. A. & Rise, L. 2005: Submarine landforms and the reconstruction of fast-flowing ice streams within a large Quaternary ice sheet: the 2500-km-long Norwegian-Svalbard margin (57–80 N). *Geological Society of America Bulletin 117*, 1033–1050.

Philippe, É. G. H., Valet, J., St-Onge, G. & Thevarasan, A. 2018: Are Palaeomagnetic Records From U-Channels Appropriate for Studies of Reversals and Excursions? *Geochemistry, Geophysics, Geosystems 19,* 4130–4142.

Philippe, É. G. H. 2019: Acquisition de l'aimantation remanente dans les sediments. PhD thesis. Université du Québec à Rimouski.

Piper, D. J. W. 1972: Sediments of the Middle Cambrian Burgess Shale, Canada. *Lethaia 5*, 169–175.

Pouderoux, H., Proust, J.-N., Lamarche, G., Orpin, A. & Neil, H. 2012: Postglacial (after 18 ka) deep-sea sedimentation along the Hikurangi subduction margin (New Zealand): Characterisation, timing and origin of turbidites. *Marine Geology 295*, 51–76.

Praeg, D. B., MacLean, B. & Sonnichsen, G. V. 2006: Quaternary geology of the northeast Baffin Island continental shelf, Cape Aston to Buchan Gulf (70° to 72° N). 98 pp. *Open File 5409*, Geological Survey of Canada.

Reimer, P. J., Bard, E., Bayliss, A., Beck, J. W., Blackwell, P. G., Bronk Ramsey, C., Buck, C. E., Edwards, R. L., Friedrich, M., Grootes, P. M., Guilderson, T. P., Haflidason, H., Hajdas, I., Hatté, C., Heaton, T. J., Hogg, A. G., Hughen, K. A., Kaiser, K. F., Kromer, B., Manning, S. W., Reimer, R. W., Richards, D. A., Scott, E. M., Southon, J. R., Turney, C. S. M. & Plicht, J. 2013: IntCal13 and MARINE13 radiocarbon age calibration curves 0-50,000 years cal BP. *Radiocarbon* 55, 1869–1887.

Roger, J., Saint-Ange, F., Lajeunesse, P., Duchesne, M. J. & St-Onge, G. 2013: Late Quaternary glacial history and meltwater discharges along the Northeastern Newfoundland Shelf. *Canadian Journal Earth Sciences 1194*.

Shanmugam, G. 2006: Deep-water processes and facies models: Implications for sandstone petroleum reservoirs. 496 pp. Elsevier, Amsterdam.

Simon, Q., St-Onge, G. & Hillaire-Marcel, C. 2012: Late Quaternary chronostratigraphic framework of deep Baffin Bay glaciomarine sediments from high-resolution palaeomagnetic data. *Geochemistry, Geophysics, Geosystems 13*.

Simon, Q., Hillaire-Marcel, C., St-Onge, G. & Andrews, J. T. 2014: North-eastern Laurentide, western Greenland and southern Innuitian ice stream dynamics during the last glacial cycle. *Journal of Quaternary Science* 29, 14–26.

Simon, Q., Thouveny, N., Bourles, D. L., Nuttin, L., Hillaire-Marcel, C. & St-Onge, G. 2016: Authigenic 10Be/9Be ratios and 10Be-fluxes (230Thxs-normalized) in central Baffin Bay sediments during the last glacial cycle: Paleoenvironmental implications. *Quaternary Science Reviews* 140, 142–162.

Snowball, I. & Muscheler, R. 2007: Palaeomagnetic intensity data: an Achilles heel of solar activity reconstructions. *The Holocene 17*, 851–859.

Snowball, I. & Sandgren, P. 2002: Geomagnetic field variations in northern Sweden during the Holocene quantified from varved lake sediments and their implications for cosmogenic nuclide production rates. *The Holocene 12*, 517–530.

St-Onge, G. Stoner, J. S. & Hillaire-Marcel, C. 2003: Holocene palaeomagnetic records from the St. Lawrence Estuary, eastern Canada: Centennial- to millennial-scale geomagnetic modulation of cosmogenic isotopes. *Earth and Planetary Science Letters 209*, 113–130.

St-Onge, G., Mulder, T., Piper, D. J. W., Hillaire-Marcel, C. & Stoner, J. S. 2004: Earthquake and flood-induced turbidites in the Saguenay Fjord (Québec): A Holocene palaeoseismicity record. *Quaternary Science Reviews 23*, 283–294.

St-Onge, G., Mulder, T., Francus, P. & Long, B. 2007: Continuous physical properties of cored marine sediments. *Developments in Marine Geology*, *1*, 63–98.

St-Onge, G. & Stoner, J. S. 2011: Palaeomagnetism Near The North Magnetic Pole. *Oceanography 24*, 162–173.

Stanley, S. & Luczaj, J. A. 2015: *Earth system history*. 624 pp. Macmillan, New York.

Stokes, C. R. & Clark, C. D. 2002: Are long subglacial bedforms indicative of fast ice flow? *Boreas 31*, 239–249.

Stokes, C. R. 2017: Deglaciation of the Laurentide Ice Sheet from the Last Glacial Maximum. *Cuadernos de Investigación Geográfica 43*, 377–428.

Stoner, J. S., Channell, J. E. T., Hillaire-Marcel, C. & Kissel, C. 2000: Geomagnetic palaeointensity and environmental record from Labrador Sea core MD95–2024: Global marine sediment and ice core chronostratigraphy for the last 110 kyr. *Earth and Planetary Science Letters 183*, 161–177.

Stoner, J. S. & St-Onge, G. 2007: Magnetic stratigraphy in palaeoceanography: reversals, excursions, palaeointensity, and secular variation. *Developments in Marine Geology 1*, 99–138.

Stow, D. A. V. & Piper, D. J. W. 1984: Deep-water fine-grained sediments: facies models. *Geological Society, London, Special Publications 15*, 611–646.

Stuiver, M., Reimer, P. J. & Reimer, R. W. 2017: CALIB 7.1. Available at: http://calib.org.

Syvitski, J. P. M. 1989: On the deposition of sediment within glacier-influenced fjords: oceanographic controls. *Marine Geology 85*, 301–329.

Syvitski, J.P. & Shaw, J. 1995: Sedimentology and geomorphology of fjords. *Developments in Sedimentology* 53, 113-178.

Syvitski, J.P., Burrell, D.C. & Skei, J.M. 2012: Fjords: processes and products. *Springer Science & Business Media*.

Tang, C. C. L., Ross, C. K., Yao, T., Petrie, B., DeTracey, B. M. & Dunlap, E. 2004: The circulation, water masses and sea-ice of Baffin Bay. *Progress in Oceanography 63*, 183–228.

Tanty, C., Valet, J., Carlut, J., Bassinot, F. & Zaragosi, S. 2016: Acquisition of detrital magnetization in four turbidites. *Geochemistry, Geophysics, Geosystems 17*, 3207–3223.

Tauxe, L. 1993: Sedimentary records of relative palaeointensity of the geomagnetic field: theory and practice. *Reviews of Geophysics 31*, 319–354.

Tauxe, L. 2010: *Essentials of palaeomagnetism*. 489 pp. University of California Press, Berkeley.

Tauxe, L. & Wu, G. 1990: Normalized remanence in sediments of the western equatorial Pacific: relative palaeointensity of the geomagnetic field? *Journal of Geophysical Research: Solid Earth 95*, 12337–12350.

Tauxe, L, Mullender, T. A. T. & Pick, T. 1996: Potbellies, wasp-waists, and superparamagnetism in magnetic hysteresis. *Journal of Geophysical Research: Solid Earth 101*, 571–583.

Toucanne, S., Zaragosi, S., Bourillet, J. F., Dennielou, B., Jorry, S. J., Jouet, G. & Cremer, M. 2012: External controls on turbidite sedimentation on the glacially-influenced Armorican margin (Bay of Biscay, western European margin). *Marine Geology 303–306*, 137–153.

Tripsanas, E. K. & Piper, D. J. W. 2008: Late Quaternary stratigraphy and sedimentology of Orphan Basin: implications for meltwater dispersal in the southern Labrador Sea. *Palaeogeography, Palaeoclimatology, Palaeoecology 260*, 521–539.

Vorren, T. O. & Laberg, J. S. 1997: Trough mouth fans—Palaeoclimate and ice-sheet monitors. Quaternary Science Reviews 16. 865–881.

Vorren, T. O., Laberg, J. S., Blaume, F., Dowdeswell, J. A., Kenyon, N. H., Mienert, J., Rumohr, J. & Werner, F. 1998: The Norwegian—Greenland Sea continental margins: morphology and late Quaternary sedimentary processes and environment. *Quaternary Science Reviews 17*, 273–302.

Winsor, K., Carlson, A. E., Klinkhammer, G. P., Stoner, J. S. & Hatfield, R. G. 2012: Evolution of the northeast Labrador Sea during the last interglaciation. *Geochemistry, Geophysics, Geosystems 13*.

Wynn, R. B. & Stow, D. A. V. 2002: Classification and characterisation of deep-water sediment waves. *Marine Geology 192*, 7–22.

Yamazaki, T., Yamamoto, Y., Acton, G., Guidry, E. P. & Richter, C. 2013: Rock-magnetic artifacts on long-term relative palaeointensity variations in sediments. *Geochemistry, Geophysics, Geosystems 14*.

Table captions

Table 1. Coordinates and properties of the coring sites.

Table 2. Radiocarbon ages from cores HU2013-029-0077, AMD0217-01 PC and AMD16-LGM-09CASQ. Radiocarbon ages were calibrated using the CALIB version 7.1 (Stuiver & Reimer

2017) and the Marine13 calibration curve (Reimer *et al.* 2013). Radiocarbon ages from core HU2013-029-0077 are from Jenner *et al.* (2018).

Figure captions

Fig. 1. A. Topographic and bathymetric map of the Baffin Bay area (Jakobsson *et al.* 2012). The red star shows the location of the sampling sites from this study: cores HU2013-029-0077 (77PC), AMD0217-01 PC and TWC (1Comp) and AMD16-LGM-09CASQ (9CASQ). The yellow star shows the location of core HU2008-029-016PC from Simon *et al.* (2012). The simplified ocean circulation is represented by the red arrows to illustrate the warm West Greenland current and by the blue arrow to represent the cold Baffin Island current. The white lines represent the ice margin at 16.5 cal. ka of the Laurentian (LIS), Innuitian (IIS) and Greenland (GIS) ice sheets according to Dyke (2004). The red square is the focus of the Fig. 1B. The dashed black line represents the maximum extent proposed in this study. The solid black line represents the maximum extent according to Dyke (2004). The red stars represent the sampling sites of cores 77PC, 9CASQ and 1Comp. Light gray lines refer to the locations of the seismic profiles shown in Figs. 3A, B and S1. The white dashed circle refers to Fig. 4. The red square is the location of the multibeam image of Figs. 5A and B. See text for details.

Fig. 2. X-radiographs and high-resolution photography of representative lithofacies from sediment cores of Home Bay TMF: AMD0217-01 PC and AMD16-LGM-09CASQ (9CASQ). A. Massive, matrix-supported diamicton facies. Complex diamicton (LF1). B. Laminated mud rich in IRD (LF2). C. Silt and sand turbidite (LF3). D. Laminated mud (LF4). E. Homogenous mud with IRD (LF5). F. Carbonate-rich bed with IRD (LF6). G. Homogenous mud without IRD (LF7). The gray dashed lines define facies changes. See Fig. 7 for facies identification legend and sediment characteristics. Add 30 cm to obtain the real depths of 1Comp.

Fig. 3. A. Acoustic (Chirp) subbottom profile over core 9CASQ site and located at the lower end of the continental slope of Home Bay. TMF near the abyssal plain. B. Huntec subbottom profile collected in 1978, showing the thick acoustically stratified interval of core 77PC located on the continental slope of Home Bay. The estimated core depths are indicated with red mark. Fig. 3B is modified from Campbell & Bennett (2014). The acoustically-transparent layers represent postglacial sediments and the high-amplitude reflections represent alternation of mud, IRD layers and turbidite.

Fig. 4. Acoustic (Chirp) subbottom profile over core AMD0217-01 PC (1Comp) site located at the lower end of the continental slope of Home Bay. The orange dashed line delimits a buried debris flow channel just aside of the core. The chaotic character of the infill on the profile is attributed to debris flow deposits. This channel is composed of a series of stacked debris flows that accumulated inside the TMF. The estimated core depths (~4 m) are indicated with the red mark.

Fig. 5. A. Angle view of the submarine morphology of the TMF showing gullies and iceberg ploughmarks. The white dashed lines correspond to the limit of 3 turbidity channels upstream of cores 9CASQ and 1Comp (AMD0217-01). The black dashed lines represent sediment transport

pathways. B. Swath bathymetry imagery showing elongated landforms interpreted as mega-scale glacial lineations (MSGLs) and iceberg ploughmarks on the shelf. See text for details.

Fig. 6. High-resolution physical, geochemical and magnetic properties of cores 77PC (A), 1Comp (B) and 9CASQ (C). See Fig. 7 for more details on facies identification. The vertical red lines delineate respectively the MAD value of 5° and the expected inclination, respectively, according to geocentric axial dipole (I_{GAD}) at the coring site. Sediments were sieved at 2 mm prior to laser size analysis and no sediment coarser than 2 mm, except for occasional pebbles, were recovered. Therefore, the >2 mm size fraction has been excluded from the grain size metrics.

Fig. 7. Sediment facies characteristics of cores 1Comp and 9CASQ. From left to right: X-radiographs, high-resolution photography, facies, sedimentary structures and processes with the depositional environment.

Fig. 8. Grain size signature (D50, D90, sorting) and inclinations of LF3 in core 9CASQ sampled in the lower continental slope of Home Bay. These trends illustrate the normal grading of a turbidite. The arrows represent the grading. The >2 mm size fraction has been excluded from the grain size metrics.

Fig. 9. A. Typical hysteresis curves and derived parameters of cores 77PC, 9CASQ and 1Comp. B. Day plot (Day *et al.* 1977). RDL = rapidly deposited layers (turbidite and debrite). C. k_{ARM} vs. k_{LF} plot representing estimated magnetic grain size for magnetite (King *et al.* 1983). Red circle represents the RDLs and black circles the remaining sediment.

Fig. 10. Schematic model for the main glaciogenic sedimentary processes inside a trough-mouth fan (TMF).

Fig. 11. Relative palaeointensity correlation. Relative palaeointensity inter-comparison for the last 45 cal. ka BP between cores 77PC (this study), 9CASQ (this study), 1Comp (this study) and RPI reference curves from the North Atlantic stack (NAPIS-75; Laj *et al.* 2000); the Baffin Bay (Core 16PC; Simon *et al.* 2012) and the Mediterranean and Somalian Stack; (Meynadier *et al.* 1992). The correlative palaeointensity features are indicated with the blue line. RDLs (e.g. debrite and turbidite) are delimited by the grey and purple square. In red, calibrated radiocarbon ages (cal. ka BP). Radiocarbon ages from core HU2013-029-0077 are from Jenner *et al.* (2018). Here, various scales are used to highlight the trends.

Supporting information

Fig. S1. Line 76029_AG_280_1730 (airgun profile) collected in 1976 on board the CCGS Hudson by the Geological Survey of Canada. This figure does not show any grounding-zone wedge (GZW) in the sector.

Fig. S2. Multibeam image and morphology of the cross-shelf trough of Home Bay visualized with the QPS Fledermaus software. The bedforms observed within the area contain iceberg ploughmarks on the cross shelf and a series of sub-parallel linear gullies going down the slope. The red star corresponds to core 1Comp (AMD0217-01) located in a trough-mouth fan (TMF).

Fig. S3. Correlation of cores 01-PC and 01-TWC (AMD0217-01 = 1Comp) based on density. Open delta symbol represents the difference between each core. The numbers represent tie-points between the two cores.

Fig. S4. RPI proxy vs. its normalizer for cores 77PC, 1Comp and 9CASQ. Red points and blue lines = RDLs. Blue points and red line = remaining sediments.

Fig. S5. RPI proxy vs. its normalizer ARM and IRM for cores 77PC, 1Comp and 9CASQ

Fig. S6. Multibeam image of the site of core 1Comp (AMD0217-01) sampled at the edge of a TMF visualized with the QPS Fledermaus software. The white dashed lines represent the delimitation of the turbidity channels.

Université du Québec à Rimouski
Institut des sciences de la mer de Rimouski

310, allée des Ursulines, C. P. 3300
Rimouski (Québec) G5L 3A1, CANADA
Téléphone : 418 724-1650
Télécopieur : 418 724-1842
Courriel : ismer@uqar.ca
www.ismer.ca

Rimouski, Canada, September 6, 2019

Prof. Jan A. Piotrowski
Editor-in-Chief
Boreas

Manuscript ID: **BOR-002-2019**

Please find attached the revised version of **manuscript no. BOR-002-2019** entitled "*Defining the maximum extent of the Laurentide Ice Sheet in Home Bay (eastern Arctic Canada) during the Last Glacial episode*" by Yan Lévesque*, Guillaume St-Onge, Patrick Lajeunesse, Pierre-Arnaud Desiage and Étienne Brouard for publication in *Boreas*. As you requested, we implemented the mark-up corrections you suggested on the two annotated files. These include formatting the text and references to the style of Boreas, as well as reducing the length of the discussion by 24 %. We also corrected all the figures as requested. Figures six and eight have been merged and table three is now figure seven. Note that the palaeomagnetic data from core 77PC are original and should be published in this manuscript. Similarly, the schematic figure with the sedimentary processes is also original and should also be published.

We wish to sincerely thank you for the time and energy used to review and edit our manuscript.

Best regards,

Yan Lévesque
*Corresponding author
Institut des sciences de la mer de Rimouski (ISMER)
Université du Québec à Rimouski
310 allée des Ursulines, Rimouski, Québec, Canada, G5L 3A1
E-mail: yan.levesque@uqar.ca

Table captions

Table 1. Coordinates and properties of the coring sites.

Table 2. Radiocarbon ages from cores HU2013-029-0077, AMD0217-01 PC and AMD16-LGM-09CASQ. Radiocarbon ages were calibrated using the CALIB version 7.1 (Stuiver & Reimer 2017) and the Marine13 calibration curve (Reimer *et al.* 2013). Radiocarbon ages from core HU2013-029-0077 are from Jenner *et al.* (2018).

Figure captions

Fig. 1. A. Topographic and bathymetric map of the Baffin Bay area (Jakobsson *et al.* 2012). The red star shows the location of the sampling sites from this study: cores HU2013-029-0077 (77PC), AMD0217-01 PC and TWC (1Comp) and AMD16-LGM-09CASQ (9CASQ). The yellow star shows the location of core HU2008-029-016PC from Simon *et al.* (2012). The simplified ocean circulation is represented by the red arrows to illustrate the warm West Greenland current and by the blue arrow to represent the cold Baffin Island current. The white lines represent the ice margin at 16.5 cal. ka of the Laurentian (LIS), Innuitian (IIS) and Greenland (GIS) ice sheets according to Dyke (2004). The red square is the focus of the Fig. 1B. The dashed black line represents the maximum extent proposed in this study. The solid black line represents the maximum extent according to Dyke (2004). The red stars represent the sampling sites of cores 77PC, 9CASQ and 1Comp. Light gray lines refer to the locations of the seismic profiles shown in Figs. 3A, B and S1. The white dashed circle refers to Fig. 4. The red square is the location of the multibeam image of Figs. 5A and B. See text for details.

Fig. 2. X-radiographs and high-resolution photography of representative lithofacies from sediment cores of Home Bay TMF: AMD0217-01 PC and AMD16-LGM-09CASQ (9CASQ). A. Massive, matrix-supported diamicton facies. Complex diamicton (LF1). B. Laminated mud rich in IRD (LF2). C. Silt and sand turbidite (LF3). D. Laminated mud (LF4). E. Homogenous mud with IRD (LF5). F. Carbonate-rich bed with IRD (LF6). G. Homogenous mud without IRD (LF7). The gray dashed lines define facies changes. See Fig. 7 for facies identification legend and sediment characteristics. Add 30 cm to obtain the real depths of 1Comp.

Fig. 3. A. Acoustic (Chirp) subbottom profile over core 9CASQ site and located at the lower end of the continental slope of Home Bay. TMF near the abyssal plain. B. Huntec subbottom profile collected in 1978, showing the thick acoustically stratified interval of core 77PC located on the continental slope of Home Bay. The estimated core depths are indicated with red mark. Fig. 3B is modified from Campbell & Bennett (2014). The acoustically-transparent layers represent postglacial sediments and the high-amplitude reflections represent alternation of mud, IRD layers and turbidite.

Fig. 4. Acoustic (Chirp) subbottom profile over core AMD0217-01 PC (1Comp) site located at the lower end of the continental slope of Home Bay. The orange dashed line delimits a buried debris flow channel just aside of the core. The chaotic character of the infill on the profile is attributed to debris flow deposits. This channel is composed of a series of stacked debris flows that accumulated inside the TMF. The estimated core depths (~4 m) are indicated with the red mark.

Fig. 5. A. Angle view of the submarine morphology of the TMF showing gullies and iceberg ploughmarks. The white dashed lines correspond to the limit of 3 turbidity channels upstream of cores 9CASQ and 1Comp (AMD0217-01). The black dashed lines represent sediment transport pathways. B. Swath bathymetry imagery showing elongated landforms interpreted as mega-scale glacial lineations (MSGLs) and iceberg ploughmarks on the shelf. See text for details.

Fig. 6. High-resolution physical, geochemical and magnetic properties of cores 77PC (A), 1Comp (B) and 9CASQ (C). See Fig. 7 for more details on facies identification. The vertical red lines delineate respectively the MAD value of 5° and the expected inclination, respectively, according to geocentric axial dipole (I_{GAD}) at the coring site. Sediments were sieved at 2 mm prior to laser size analysis and no sediment coarser than 2 mm, except for occasional pebbles, were recovered. Therefore, the >2 mm size fraction has been excluded from the grain size metrics.

Fig. 7. Sediment facies characteristics of cores 1Comp and 9CASQ. From left to right: X-radiographs, high-resolution photography, facies, sedimentary structures and processes with the depositional environment.

Fig. 8. Grain size signature (D50, D90, sorting) and inclinations of LF3 in core 9CASQ sampled in the lower continental slope of Home Bay. These trends illustrate the normal grading of a turbidite. The arrows represent the grading. The >2 mm size fraction has been excluded from the grain size metrics.

Fig. 9. A. Typical hysteresis curves and derived parameters of cores 77PC, 9CASQ and 1Comp. B. Day plot (Day *et al.* 1977). RDL = rapidly deposited layers (turbidite and debrite). C. k_{ARM} vs. k_{LF} plot representing estimated magnetic grain size for magnetite (King *et al.* 1983). Red circle represents the RDLs and black circles the remaining sediment.

Fig. 10. Schematic model for the main glaciogenic sedimentary processes inside a trough-mouth fan (TMF).

Fig. 11. Relative palaeointensity correlation. Relative palaeointensity inter-comparison for the last 45 cal. ka BP between cores 77PC (this study), 9CASQ (this study), 1Comp (this study) and RPI reference curves from the North Atlantic stack (NAPIS-75; Laj *et al.* 2000); the Baffin Bay (Core 16PC; Simon *et al.* 2012) and the Mediterranean and Somalian Stack; (Meynadier *et al.* 1992). The correlative palaeointensity features are indicated with the blue line. RDLs (e.g. debrite and turbidite) are delimited by the grey and purple square. In red,

calibrated radiocarbon ages (cal. ka BP). Radiocarbon ages from core HU2013-029-0077 are from Jenner *et al.* (2018). Here, various scales are used to highlight the trends.

Supporting information

Fig. S1. Line 76029_AG_280_1730 (airgun profile) collected in 1976 on board the CCGS Hudson by the Geological Survey of Canada. This figure does not show any grounding-zone wedge (GZW) in the sector.

Fig. S2. Multibeam image and morphology of the cross-shelf trough of Home Bay visualized with the QPS Fledermaus software. The bedforms observed within the area contain iceberg ploughmarks on the cross shelf and a series of sub-parallel linear gullies going down the slope. The red star corresponds to core 1Comp (AMD0217-01) located in a trough-mouth fan (TMF).

Fig. S3. Correlation of cores 01-PC and 01-TWC (AMD0217-01 = 1Comp) based on density. Open delta symbol represents the difference between each core. The numbers represent tie-points between the two cores.

Fig. S4. RPI proxy vs. its normalizer for cores 77PC, 1Comp and 9CASQ. Red points and blue lines = RDLs. Blue points and red line = remaining sediments.

Fig. S5. RPI proxy vs. its normalizer ARM and IRM for cores 77PC, 1Comp and 9CASQ

Fig. S6. Multibeam image of the site of core 1Comp (AMD0217-01) sampled at the edge of a TMF visualized with the QPS Fledermaus software. The white dashed lines represent the delimitation of the turbidity channels.

Core	Latitude (°N)	Longitude (°W)	Location	Water depth (m)	Length (cm)
HU2013-029-0077	69.31	63.79	Slope	1153	597
AMD16-LGM-09 CASQ	68.28	64.56	Slope (TMF)	1220	554
AMD0217-01 PC/TWC	69.24	64.43	Slope (TMF)	1076	350/152
Composite	69.24	64.43	Slope (TMF)	1076	380

Core	Depth (cm)	Material	Conventional age	Calibrated age (cal. a BP)	Lab. number
77PC	142	Mixed benthic foraminifera	10 550±40	11 327	OS-117723
	205	Mixed planktonic foraminifera	12 750±55	14 013	OS-118359
	644 (core catcher)	Neogloboquadrina pachyderma	37 900±1600	41 461	OS-UCIAMS 181265
9CASQ	465	Mixed benthic and planktonic foraminifera	35 160±760	39 024	ECHo 2458
01-PC	109 (not valid)	Mixed benthic and planktonic foraminifera	10 180±1490	11 029	ECHo 2559
	135	Mixed benthic and planktonic foraminifera	12 820±60	14 088	ECHo 2558

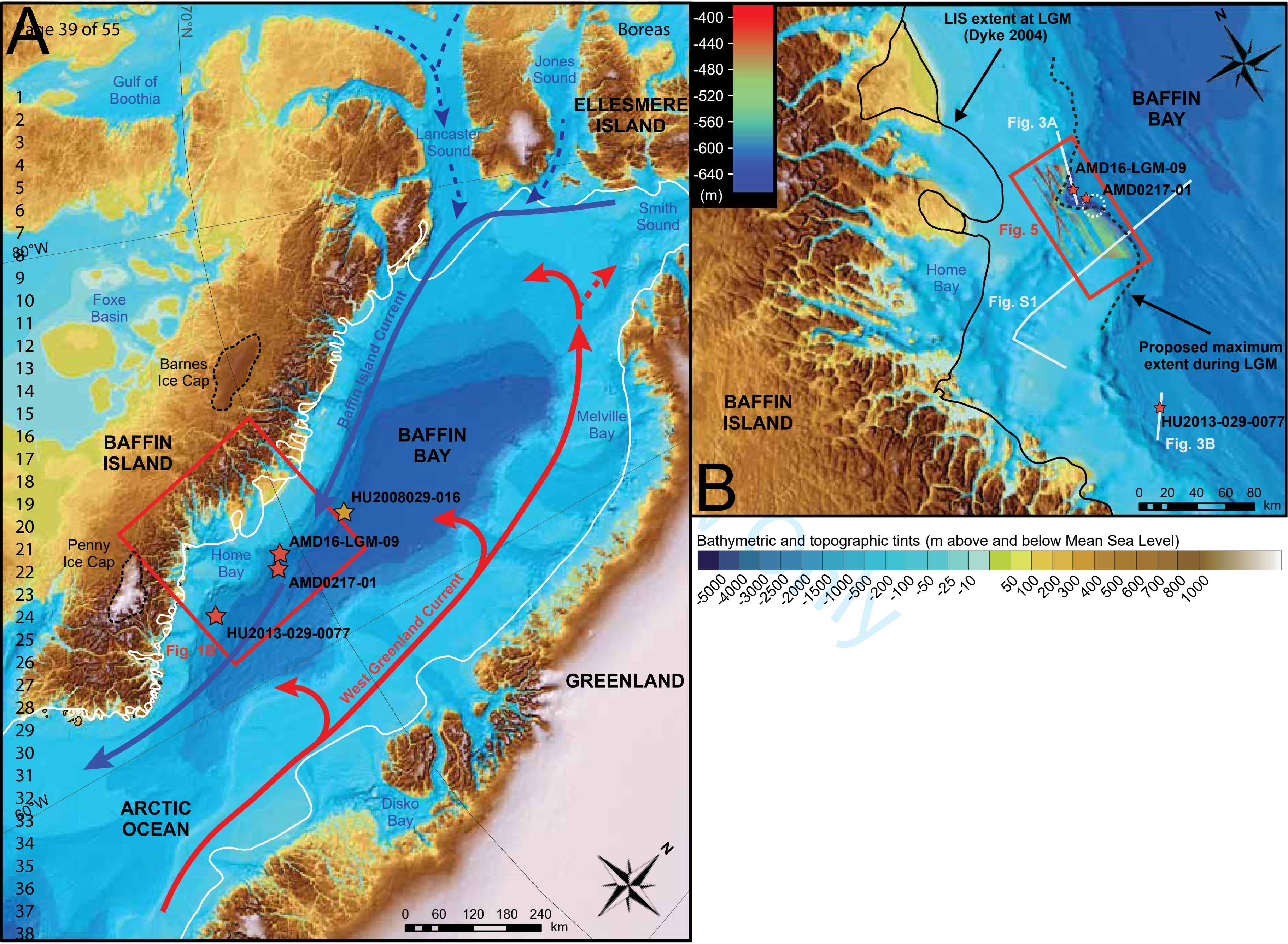
A
70°N
Boreas
Gulf of Boothia
Jones Sound
Lancaster Sound
ELLESMERE ISLAND
Smith Sound
80°W
Foxe Basin
Barnes Ice Cap
Baffin Island Current
BAFFIN BAY
Melville Bay
BAFFIN ISLAND
HU2008029-016
AMD16-LGM-09
Penny Ice Cap
Home Bay
AMD0217-01
HU2013-029-0077
Fig. 1B
West Greenland Current
GREENLAND
60°W
ARCTIC OCEAN
Disko Bay
N
0 60 120 180 240 km
B
-400
-440
-480
-520
-560
-600
-640
(m)
LIS extent at LGM (Dyke 2004)
N
BAFFIN BAY
Fig. 3A
AMD16-LGM-09
AMD0217-01
Fig. 5
Home Bay
Fig. S1
Proposed maximum extent during LGM
BAFFIN ISLAND
HU2013-029-0077
Fig. 3B
0 20 40 60 80 km
Bathymetric and topographic tints (m above and below Mean Sea Level)
-5000 -4000 -3000 -2500 -2000 -1500 -1000 -500 -200 -100 -50 -25 -10 50 100 200 300 400 500 600 700 800 1000

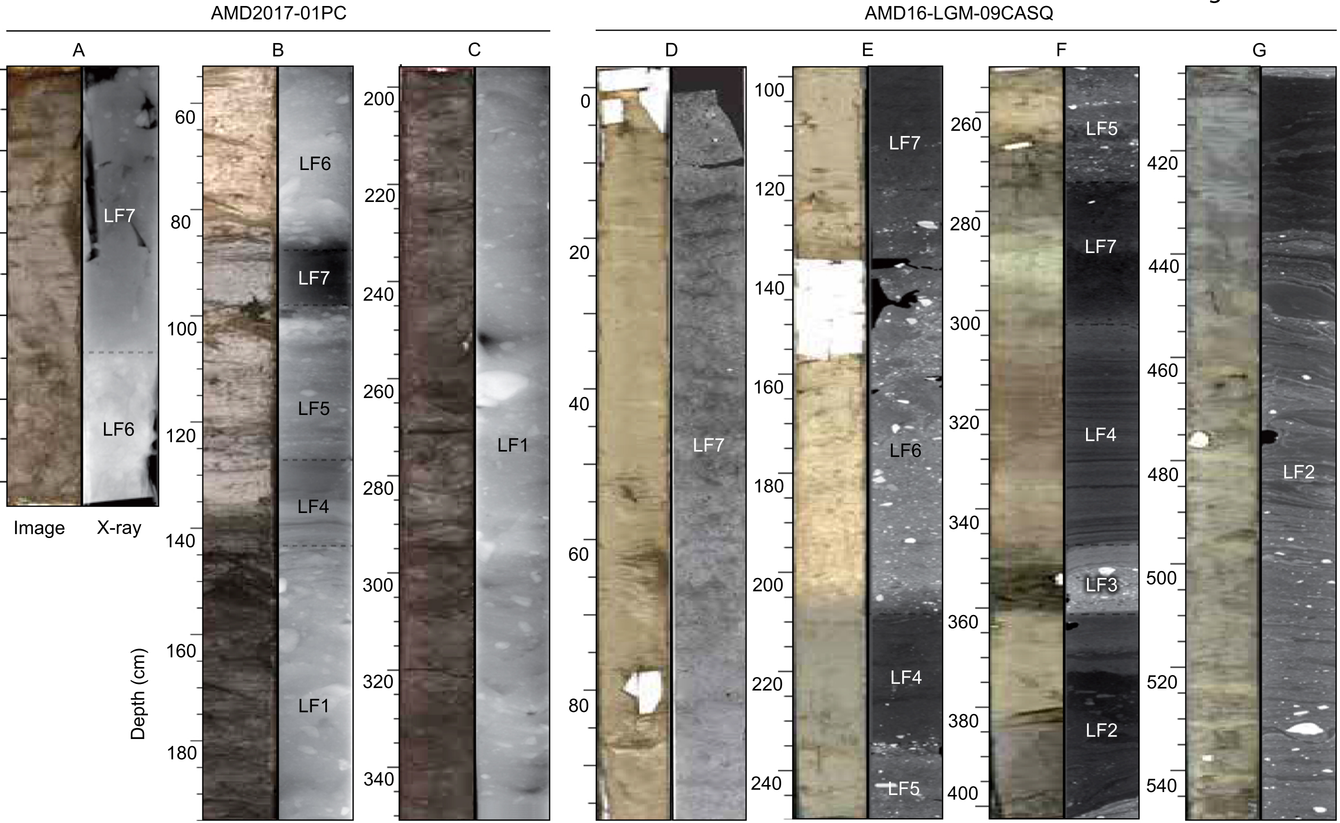
AMD2017-01PC
AMD16-LGM-09CASQ
A
B
C
D
E
F
G
LF7
LF6
LF7
LF6
LF5
LF4
LF1
LF1
LF7
LF7
LF6
LF4
LF5
LF5
LF7
LF4
LF3
LF2
LF2
Image
X-ray
Depth (cm)
0
20
40
60
80
100
120
140
160
180
200
220
240
260
280
300
320
340
0
20
40
60
80
100
120
140
160
180
200
220
240
260
280
300
320
340
360
380
400
420
440
460
480
500
520
540

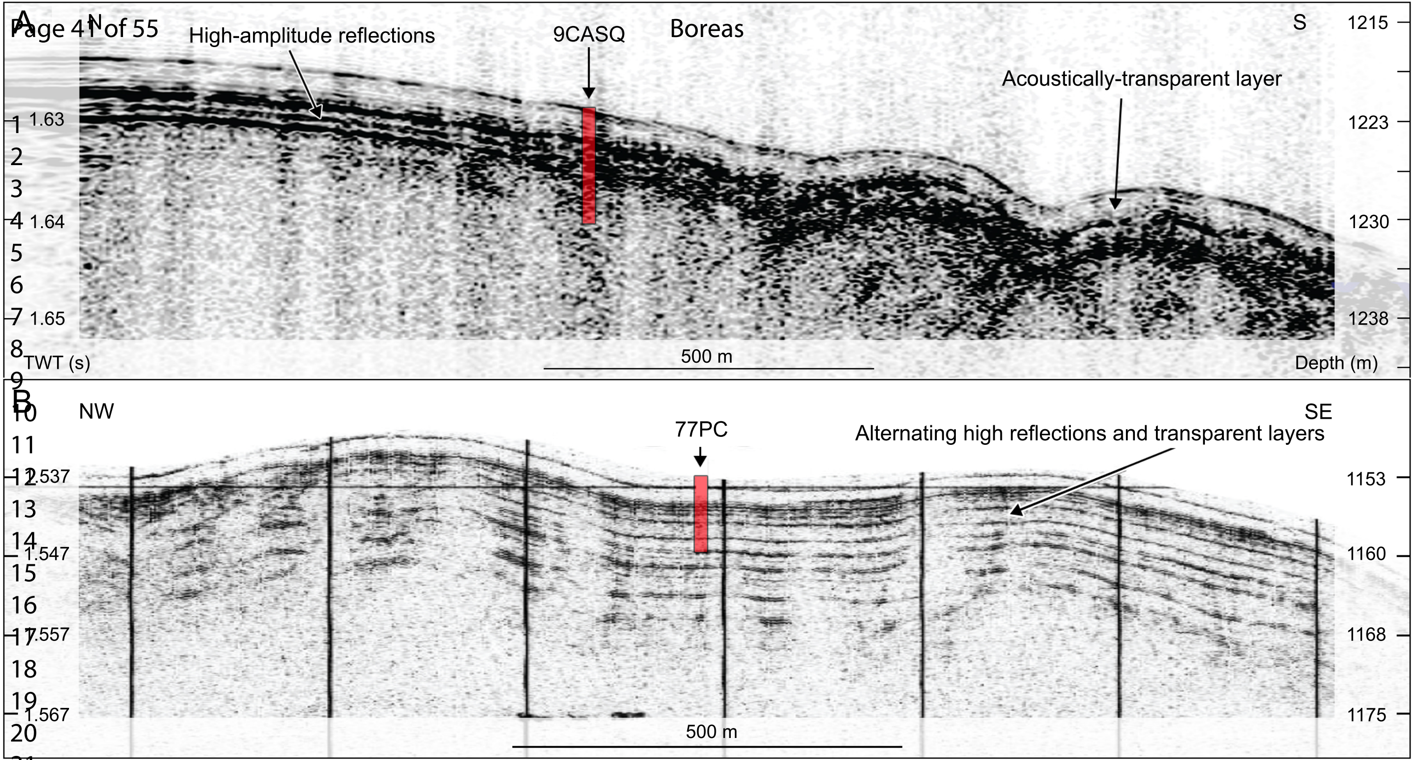
A
N
High-amplitude reflections
9CASQ
Boreas
S
Acoustically-transparent layer
1.63
1.64
1.65
TWT (s)
500 m
Depth (m)
1215
1223
1230
1238
B
NW
77PC
SE
Alternating high reflections and transparent layers
1.537
1.547
1.557
1.567
1153
1160
1168
1175
500 m

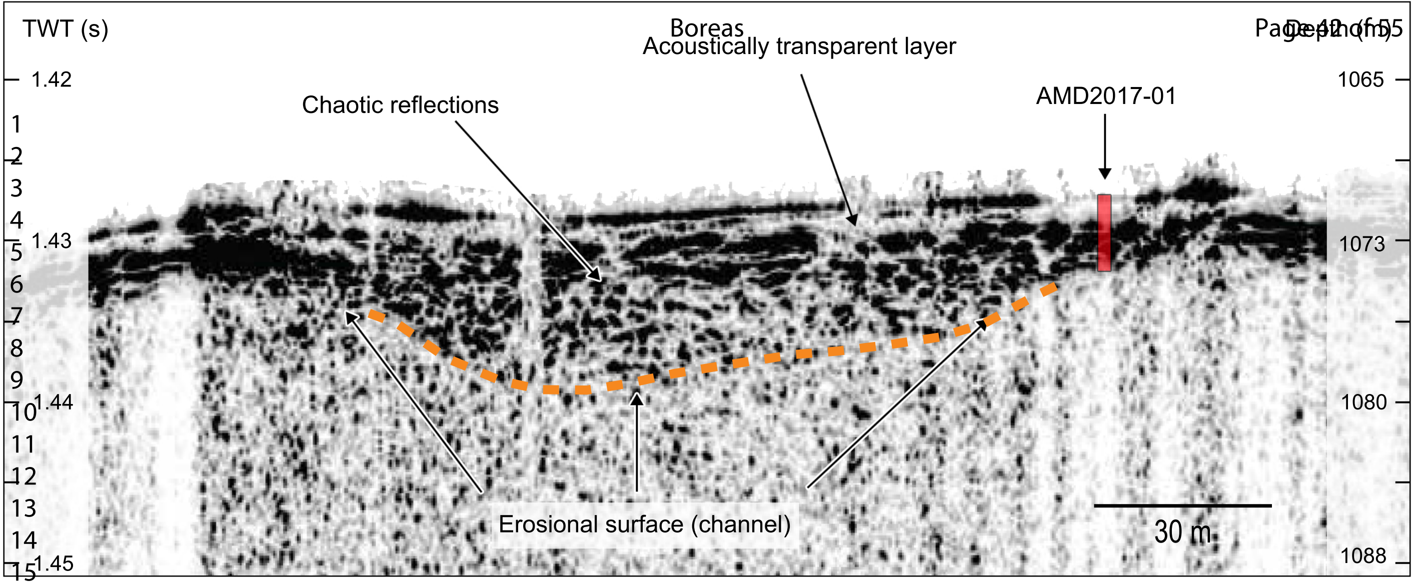
TWT (s)
Depth (m)
1.42
1.43
1.44
1.45
1065
1073
1080
1088
Acoustically transparent layer
Chaotic reflections
AMD2017-01
Erosional surface (channel)
30 m

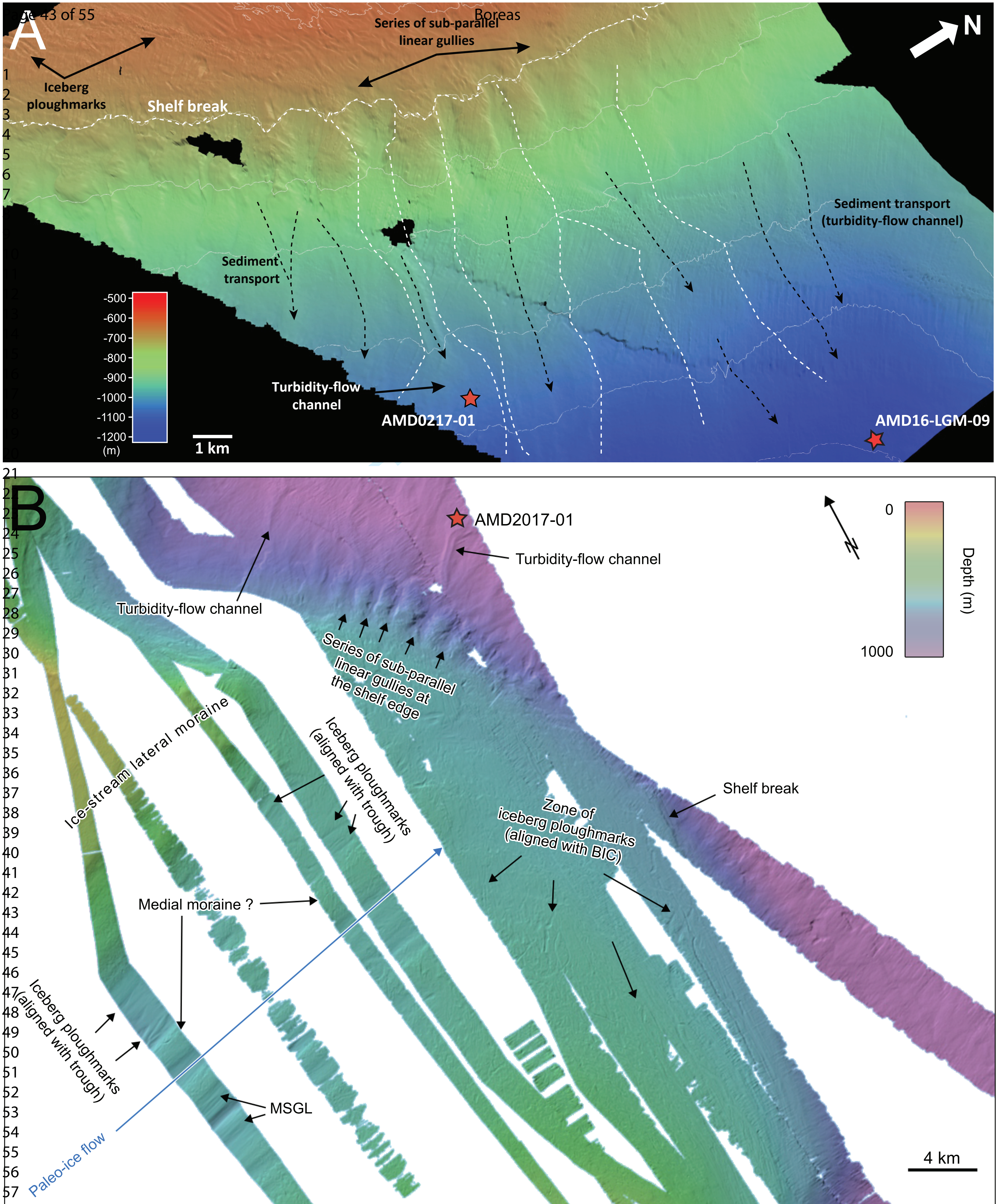
A
N
Series of sub-parallel linear gullies
Iceberg ploughmarks
Shelf break
Sediment transport
Sediment transport (turbidity-flow channel)
Turbidity-flow channel
AMD0217-01
AMD16-LGM-09
-500
-600
-700
-800
-900
-1000
-1100
-1200
(m)
1 km
B
AMD2017-01
Turbidity-flow channel
Turbidity-flow channel
0
1000
Depth (m)
Series of sub-parallel linear gullies at the shelf edge
Ice-stream lateral moraine
Iceberg ploughmarks (aligned with trough)
Shelf break
Zone of iceberg ploughmarks (aligned with BIC)
Medial moraine ?
Iceberg ploughmarks (aligned with trough)
MSGL
Paleo-ice flow
4 km

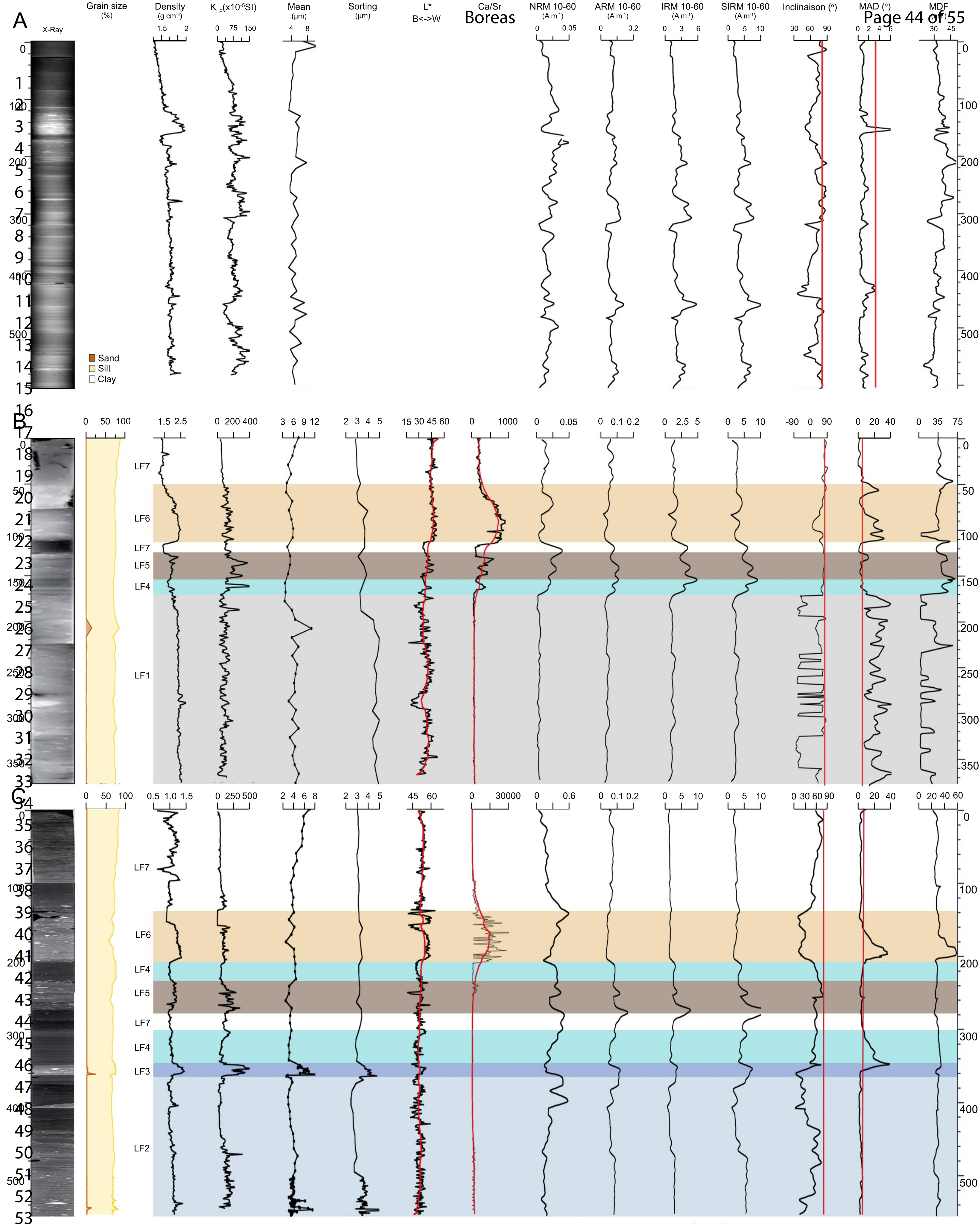
A
B
C
X-Ray
Grain size (%)
Density (g cm⁻³)
K_LF (x10⁻⁵SI)
Mean (μm)
Sorting (μm)
L* B<->W
Ca/Sr
NRM 10-60 (A m⁻¹)
ARM 10-60 (A m⁻¹)
IRM 10-60 (A m⁻¹)
SIRM 10-60 (A m⁻¹)
Inclinaison (°)
MAD (°)
MDF (mT)
Sand
Silt
Clay
LF1
LF2
LF3
LF4
LF5
LF6
LF7

X-ray	Image	Facies	Sedimentary Structures	Sedimentary Processes
055 cm 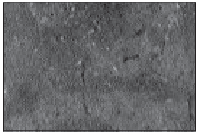 060 cm	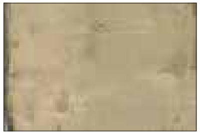	Homogenous mud without IRD (LF7)	Bioturbated grayish to brownish mud without IRD. No apparent structure are observed.	Hemipelagic sedimentation (postglacial).
179 cm 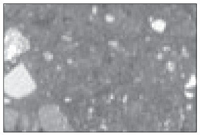 183 cm	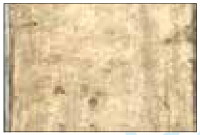	Rich carbonate bed with IRD (LF6)	Light olive brown sandy mud and pebbly mud rich in IRD.	Hemipelagic sedimentation with frequent IRD (deglacial/postglacial).
250 cm 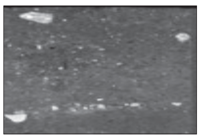 260 cm		Homogenous mud with IRD (LF5)	Dark grayish brown silty mud with IRD. No apparent structures are observable.	
343 cm 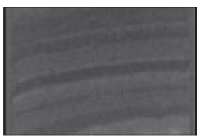 347 cm		Laminated mud (LF4)	Dark grayish brown rhytmic succession of mud and silt laminae.	Meltwater plume, turbidity current and possible bottom current influence (deglacial).
354 cm 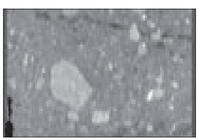 360 cm		Silt and sand turbidite (LF3)	Dense and very dark gray silt and fine sand with clast.	Turbidity current (glacial environment).
490 cm 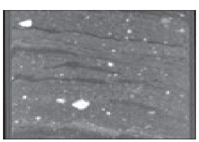 498 cm		Laminated mud rich in IRD (LF2)	Succession of dark gray to dark grayish brown silty laminated mud rich in IRD.	Meltwater plume, ice rafting and turbidity current (glacial environment).
258 cm  273 cm		Complex diamicton (LF1)	Massive, matrix-supported diamict facies. Very dense, black and coarse-grained sediment mixed with a fine-grained matrix.	Glacigenic debris flow (glacial environment).

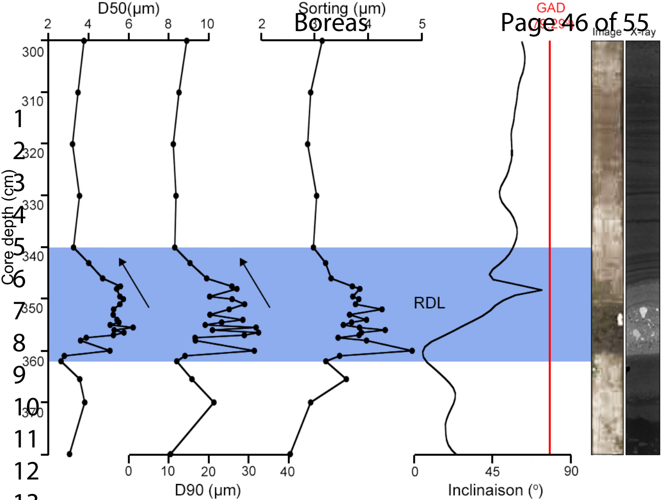
D50(µm)
2 4 6 8 10
Sorting (µm)
2 3 4 5
GAD
Image
X-ray
Core depth (cm)
300
310
320
330
340
350
360
370
RDL
0 10 20 30 40
D90 (µm)
0 45 90
Inclinaison (°)

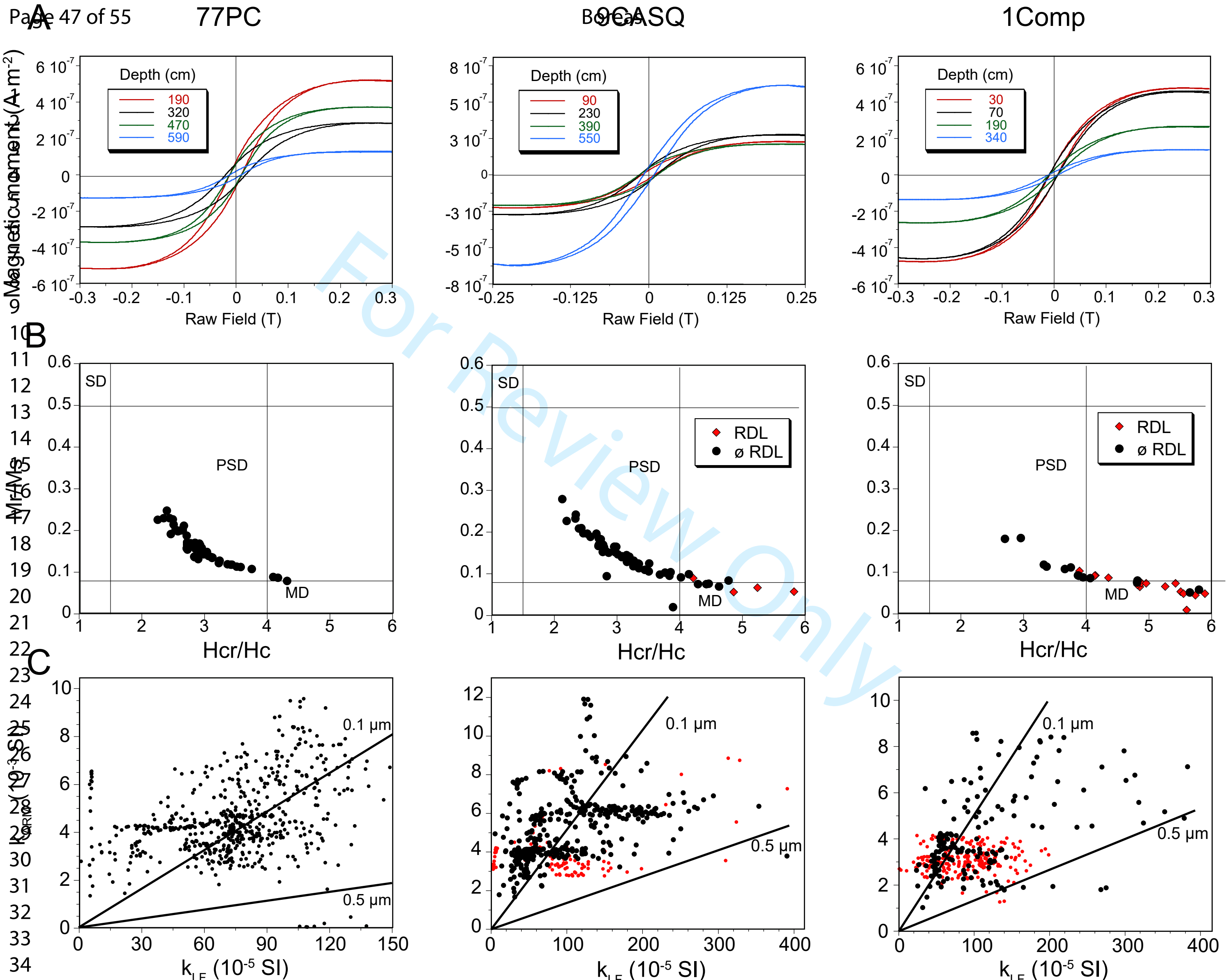
A
77PC
9CASQ
1Comp
Depth (cm)
190
320
470
590
90
230
390
550
30
70
190
340
Magnetic moment (A m-2)
Raw Field (T)
B
SD
PSD
MD
RDL
ø RDL
Mr/Ms
Hcr/Hc
C
0.1 µm
0.5 µm
kLF (10-5 SI)

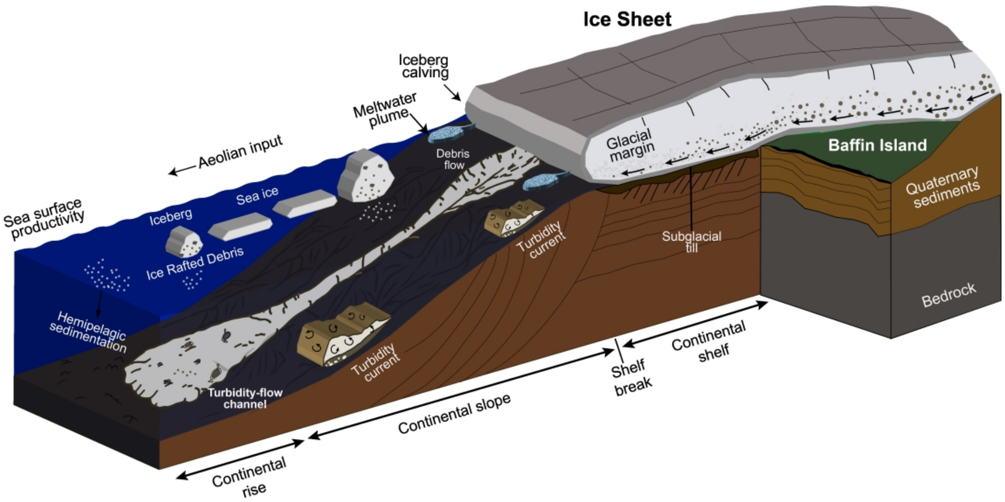
Ice Sheet
Iceberg calving
Meltwater plume
Aeolian input
Debris flow
Sea surface productivity
Iceberg
Sea ice
Ice Rafted Debris
Hemipelagic sedimentation
Turbidity-flow channel
Turbidity current
Turbidity current
Glacial margin
Baffin Island
Quaternary sediments
Subglacial till
Bedrock
Continental shelf
Shelf break
Continental slope
Continental rise

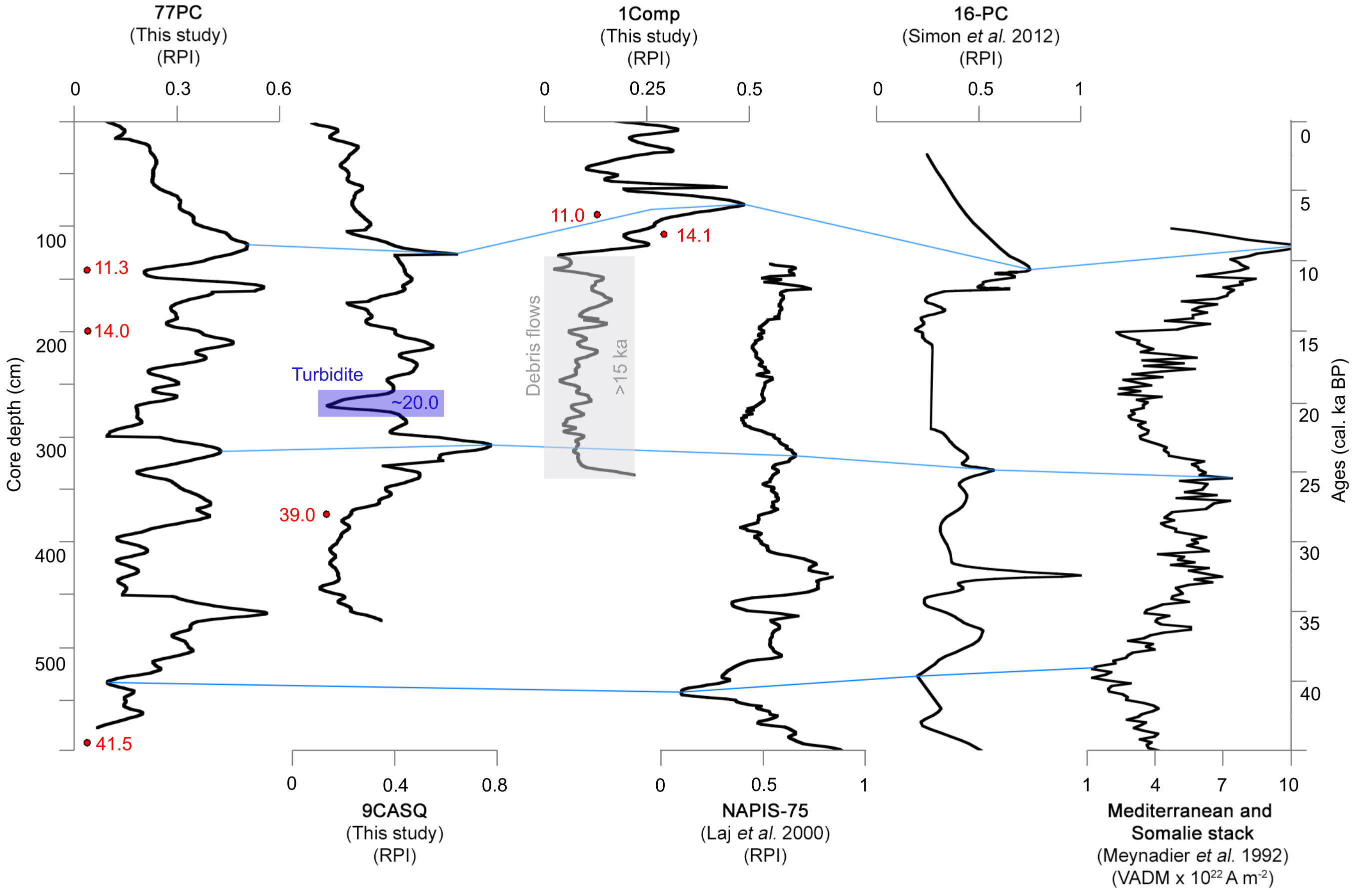
77PC
(This study)
(RPI)
0 0.3 0.6
1Comp
(This study)
(RPI)
0 0.25 0.5
16-PC
(Simon et al. 2012)
(RPI)
0 0.5 1
Core depth (cm)
100 200 300 400 500
11.3
14.0
41.5
11.0
14.1
39.0
Turbidite
~20.0
Debris flows
>15 ka
Ages (cal. ka BP)
0 5 10 15 20 25 30 35 40
0 0.4 0.8
9CASQ
(This study)
(RPI)
0 0.5 1
NAPIS-75
(Laj et al. 2000)
(RPI)
1 4 7 10
Mediterranean and
Somalie stack
(Meynadier et al. 1992)
(VADM x 10²² A m⁻²)

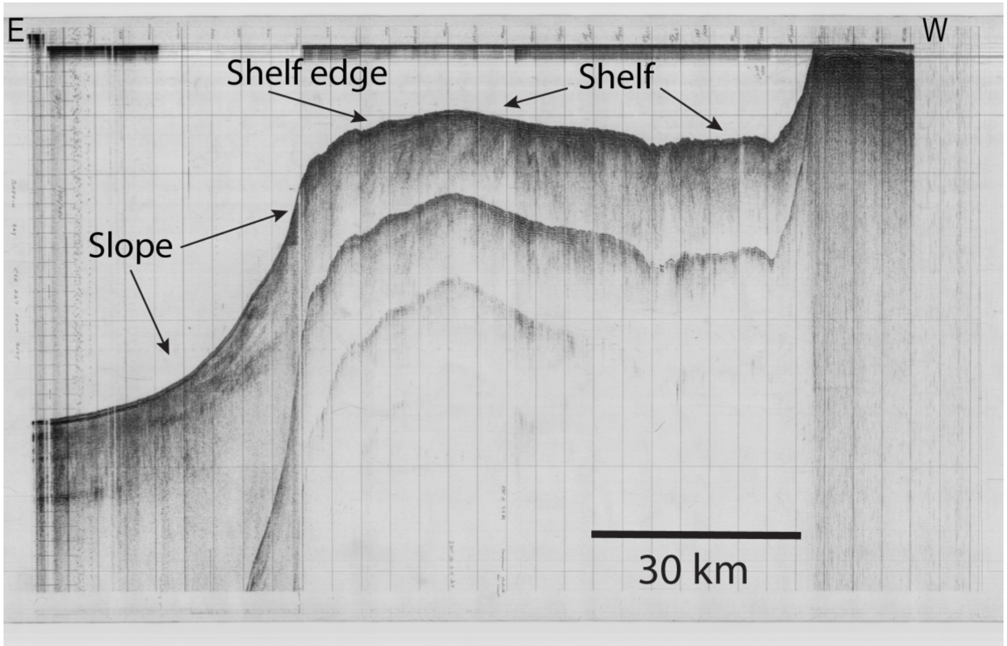
E
W
Shelf edge
Shelf
Slope
30 km

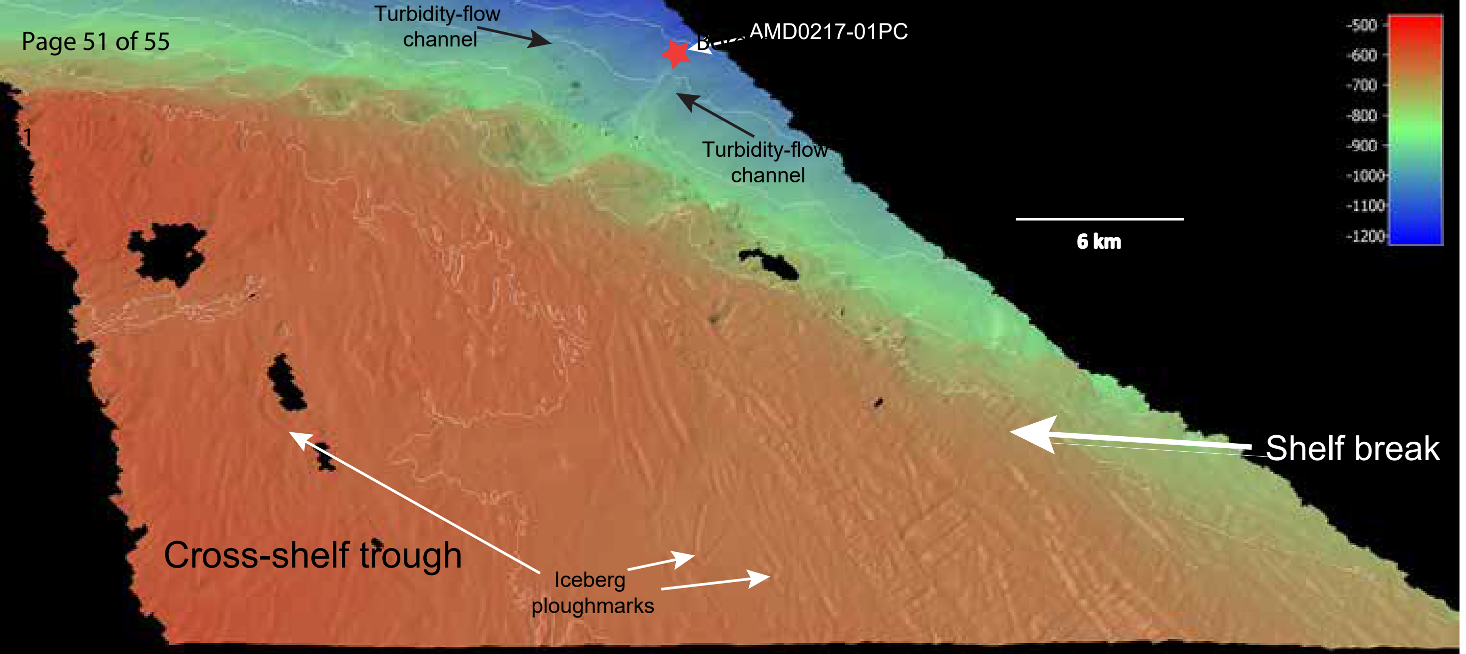
Turbidity-flow channel
AMD0217-01PC
Turbidity-flow channel
-500
-600
-700
-800
-900
-1000
-1100
-1200
6 km
Shelf break
Cross-shelf trough
Iceberg ploughmarks

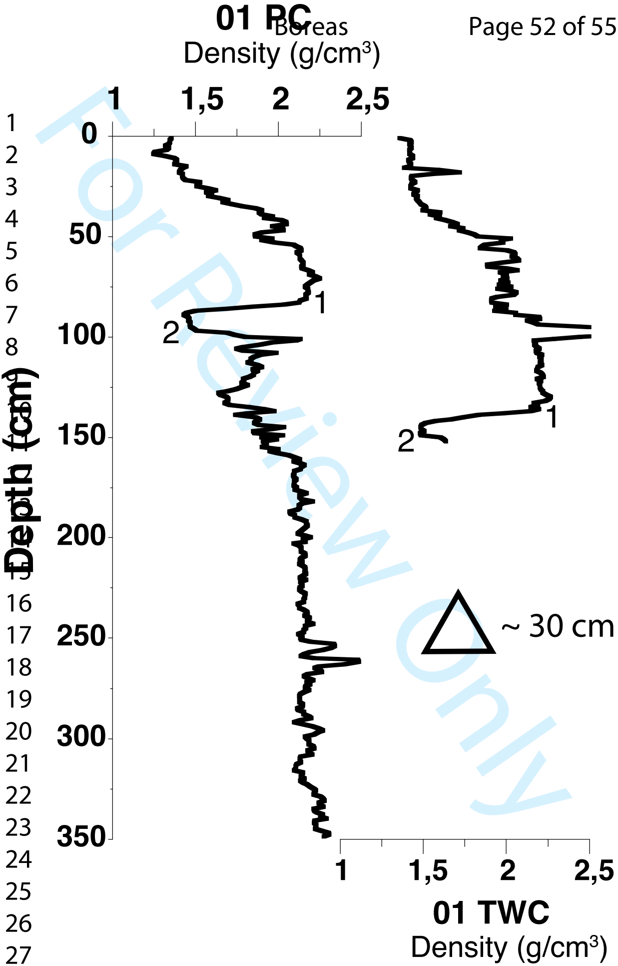
01 RC
Density (g/cm³)
1
1,5
2
2,5
0
50
100
150
200
250
300
350
Depth (cm)
1
2
1
2
~ 30 cm
1
1,5
2
2,5
01 TWC
Density (g/cm³)

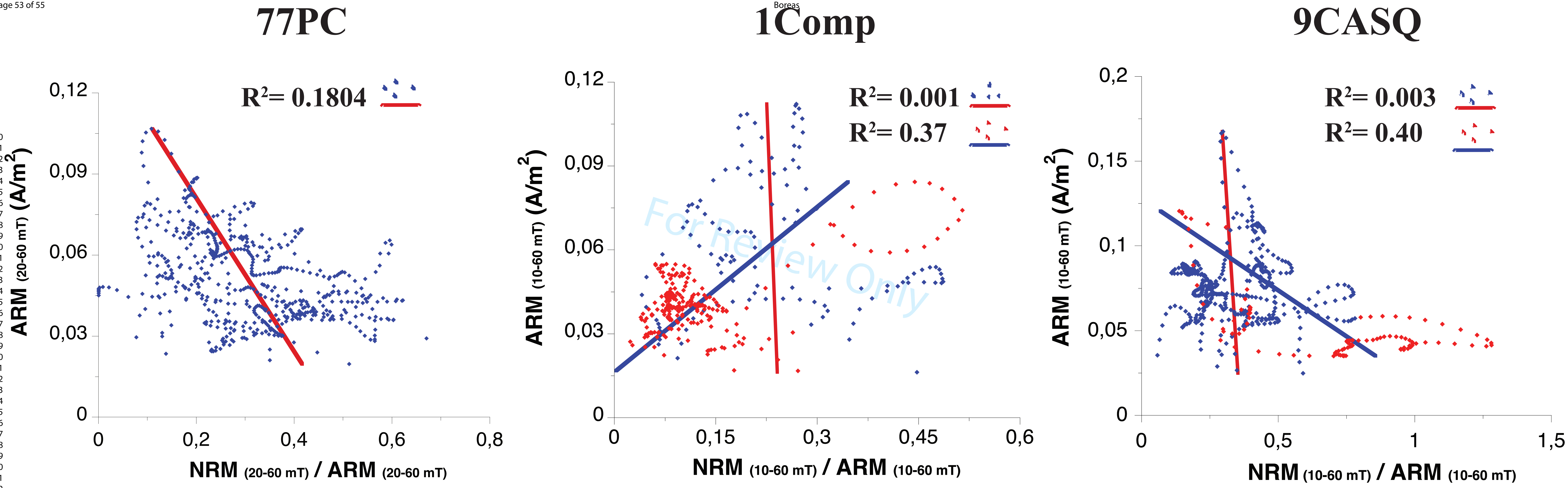
77PC
R²= 0.1804
ARM (20-60 mT) (A/m²)
0,12
0,09
0,06
0,03
0
0
0,2
0,4
0,6
0,8
NRM (20-60 mT) / ARM (20-60 mT)
1Comp
R²= 0.001
R²= 0.37
ARM (10-60 mT) (A/m²)
0,12
0,09
0,06
0,03
0
0
0,15
0,3
0,45
0,6
NRM (10-60 mT) / ARM (10-60 mT)
9CASQ
R²= 0.003
R²= 0.40
ARM (10-60 mT) (A/m²)
0,2
0,15
0,1
0,05
0
0
0,5
1
1,5
NRM (10-60 mT) / ARM (10-60 mT)

77PC

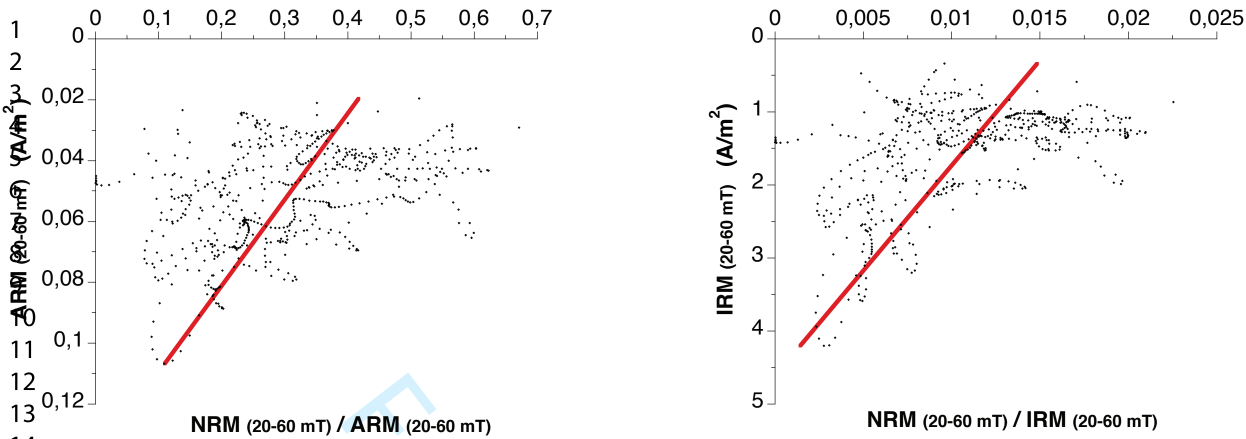

1Comp

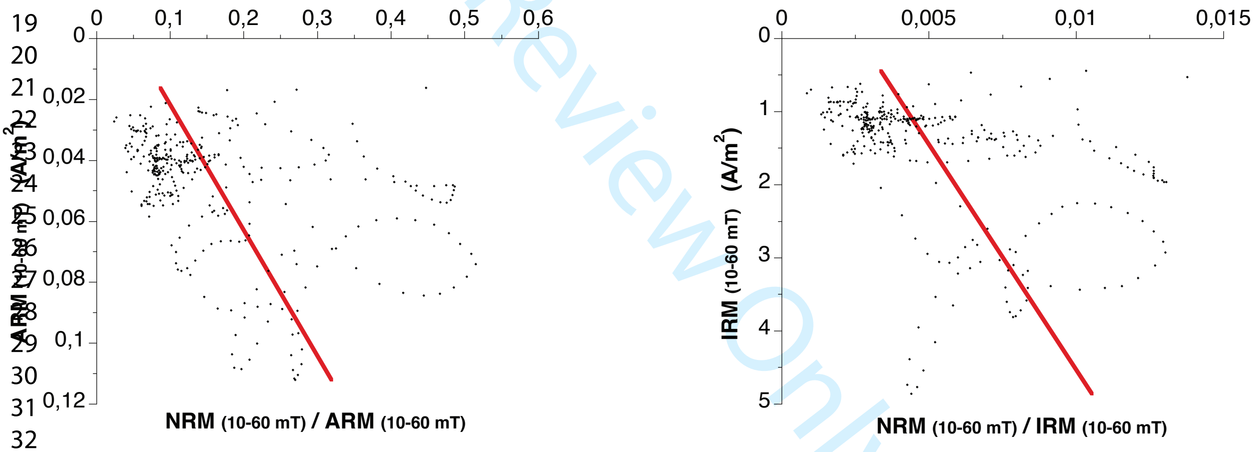

9CASQ

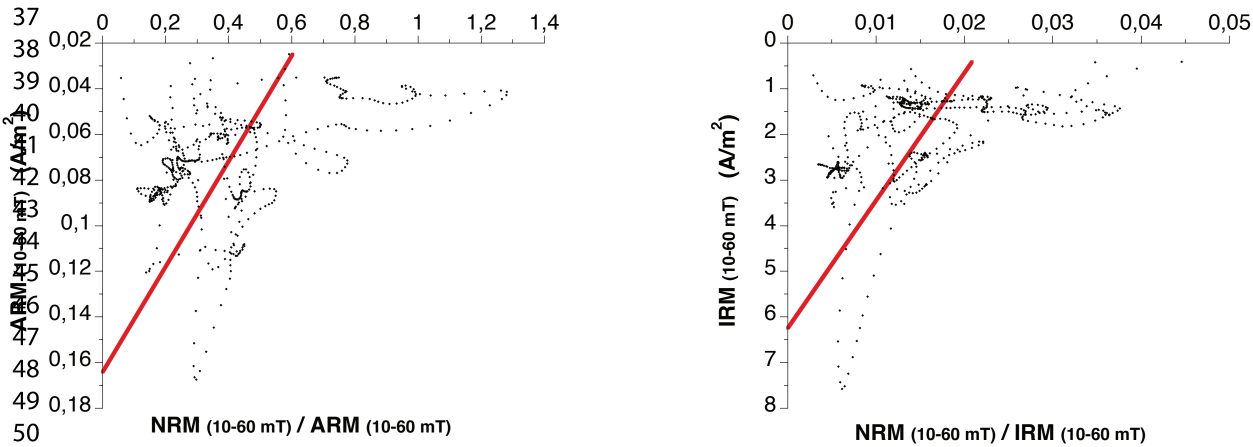

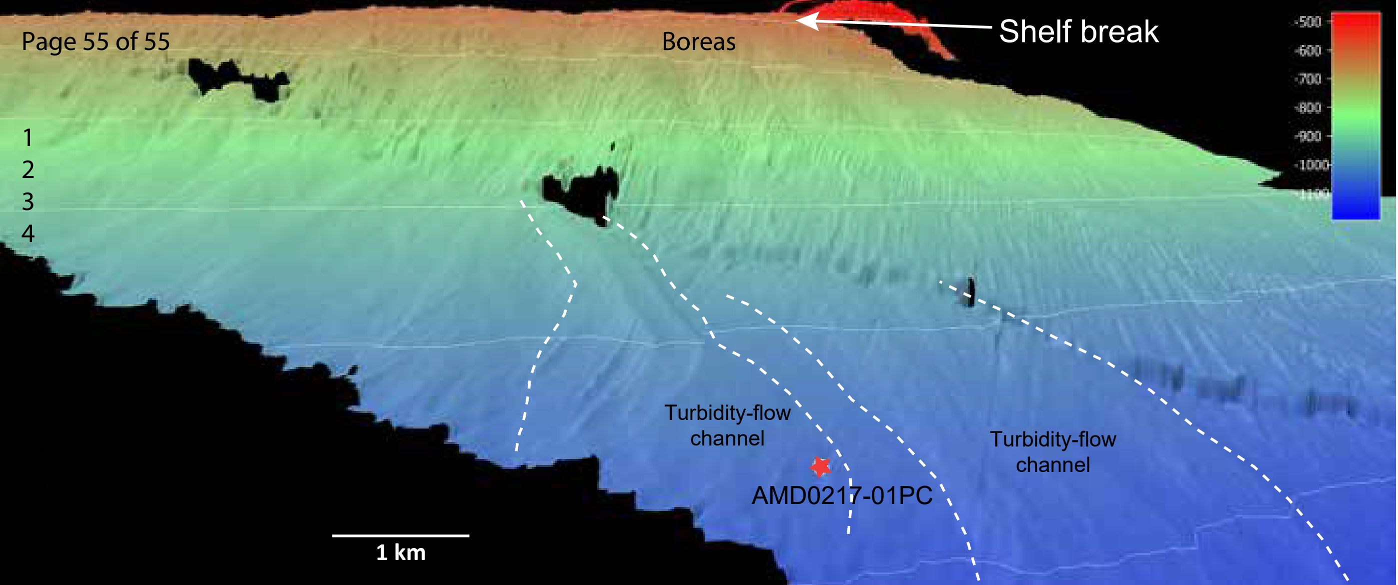
Boreas
Shelf break
-500
-600
-700
-800
-900
-1000
Turbidity-flow channel
Turbidity-flow channel
AMD0217-01PC
1 km